

# Burdening (or not) gravitational waves in the presence of primordial black holes

Mathieu Gross\* and Yann Mambrini†

Université Paris-Saclay, CNRS/IN2P3, IJCLab, 91405 Orsay, France

Md Riajul Haque‡

Physics and Applied Mathematics Unit, Indian Statistical Institute, 203 B.T. Road, Kolkata 700108, India

We present the spectrum of primordial gravitational wave (GW) expected from the presence of primordial black holes (PBH) and inflaton in the early Universe. For the first time, we combine the waves produced by the PBH decay, with their density fluctuation counterpart, as well as their effects on the GW produced by the inflaton *after* (high frequency modes) and *before* (low frequency modes) the end of inflation. We generalize our study for a potential  $V(\phi) \propto \phi^k$  during reheating. We also extend our study, taking into account a possible memory burden effect to see how it can affect the shape of the spectrum.

## I. INTRODUCTION AND CONCLUSION

The discovery of gravitational waves (GW) at the Hertz scale in 2015 [1–3] opened a new window in the physics of black holes [4–7]. Several experiments like the Einstein Telescope [8] or e-LISA [9] proposed to cover a larger range of frequencies, down to the micro-Hertz, whereas pulsar timing array already analyzed secondary GW generated by hypothetical PBH down to the nanohertz [10–15]. However, another type of gravitational waves is also of great interest to study the cosmology in early Universe, at larger frequencies. Indeed, different gravitational sources exist from the inflationary era to the BBN epoch.

The high frequency GW spectrum we obtained, taking into account the two main sources in the early Universe (inflaton and PBH) is represented in Fig. 1. It shows the relic density observed today,  $\Omega_{GW}h^2$  as function of the present frequency  $f_0$ . As an illustration, this spectrum was obtained for a population of 1 gram PBHs, responsible for the reheating in the Universe [16]. We incorporate a possible memory burden effect [17–19] through the light dashed line. We also display some sensitivity prospects for future gravitational wave observatories such as BBO [20, 21], LISA [9] and Einstein telescope (ET) [22–24] as well as current and projected experimental constraints from CMB measurements (Planck, COrE/Euclid and CVL) [25–27].

Our paper is organized to explain the features of the GW spectrum, from the lower frequencies to the highest ones. On the far left, the flat part of the spectrum labeled  $A_1$ , corresponds to the primordial GW modes which have entered in the horizon *after* the end of reheating, *ie.* during the radiation dominated era. After

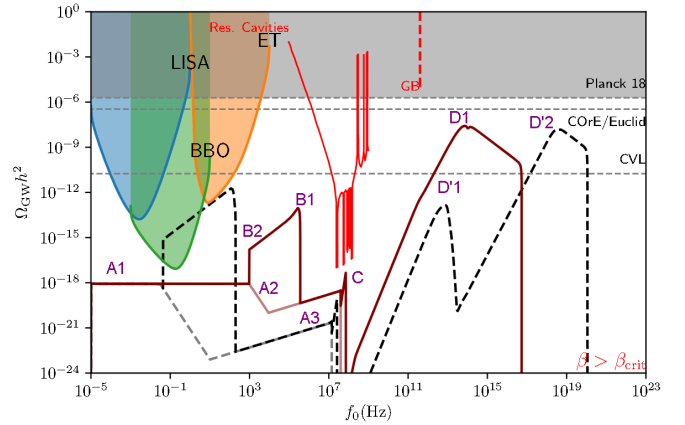


Figure 1. Minimal Gravitational wave spectra coming from a PBH reheating phase after inflation, with an inflaton potential  $V(\phi) \propto \phi^6$  during reheating. The thick red curve corresponds to  $\beta = 10^{-5}$  while the dashed black one takes care of the memory burden effect, Eq. (12), with  $n = 1$  and  $\beta = 10^{-8}$ . For both curves  $M_{BH} = 1$  g. The regions  $A_i$ ,  $B_i$ ,  $C$  and  $D_i$  are described in the text.

reminding the basis of PBH physics, and the subtleties of the burden effect in section II, we explain this range of frequencies in section III.A.

Following the red (full) line, we then observe a peak between  $f_0 \simeq 1 - 100$  kHz, labeled  $B_2$  and  $B_1$ . These GW are generated by the density fluctuations of the PBH background. The peak frequency corresponds roughly to the mean separation between PBHs at evaporation time, whereas the lower one to the size of the Universe at the evaporation time. This mechanism is described in section V.

After the peak, the density of GW increases as a power law with the frequency in the region  $A_3$ , between  $\sim 10^5$  and  $\sim 10^7$  Hz. These GW are the modes entering in

\* mathieu.gross@ijclab.in2p3.fr

† yann.mambrini@ijclab.in2p3.fr

‡ riaj.0009@gmail.com

the horizon *before* the PBHs decay, when the Universe is still dominated by the oscillations of the inflaton field  $\phi$ , whose equation of state is  $P_\phi = w_\phi \rho_\phi$ . We took  $w_\phi = \frac{1}{2}$  for the illustration, which we explain in section III C.

The brutal cut in the spectrum at  $f_0 \simeq 10^7$  Hz, region C, corresponds to the modes which never exited the horizon during inflation. They can be interpreted as sourced by prompt inflaton scattering, as we explain in section IV.

Finally, around  $f_0 \simeq 10^{15}$  Hz, we observe a (double) peak labeled  $D_1$  ( $D'_1$  and  $D'_2$ ) which is generated by the gravitons directly produced through the evaporation of the (burdened) PBH. This happens at frequencies corresponding roughly to the redshifted Hawking temperature, and is explained in section VI. We then conclude in section VII.

## II. THE PHYSICS OF PBH

The presence of primordial black holes can drastically change the physics in the early Universe, particularly with regard to GW. They can play a role in the expansion rate if they come to dominate over the inflaton field [28], be the main source the reheating process if they lived sufficiently long enough [16], and even populate the dark component [28] or induce leptogenesis [29]. They also have the possibility to generate gravitational wave [30–34], or modify their spectrum. See [35] and [36] for recent reviews on the subject. All these effects depend on the evaporation process, which is also up for discussion, especially considering memory burden corrections to the semi-classical approach [37].

### A. The semi-classical approach

From the seminal work of S Hawking in 1974 [38], it is known that a black hole can “explode”, releasing its entropy under the form of the Hawking radiation [39], described by the equation

$$\frac{dM_{\text{BH}}}{dt} = -\epsilon \frac{M_P^4}{M_{\text{BH}}^2}, \quad (1)$$

with  $\epsilon = \frac{27}{4} \frac{\pi g_*(T_{\text{BH}})}{480}$ , where  $g_*(T_{\text{BH}})$  is the number of degrees of freedom associated with the PBH temperature, and  $M_P = 1/\sqrt{8\pi G} \simeq 2.4 \times 10^{18}$  GeV is the reduced Planck mass. The factor  $27/4$  [40] accounts for the grey-body factor<sup>1</sup>. This energy loss corresponds to the Hawking temperature

$$T_{\text{BH}} = \frac{M_P^2}{M_{\text{BH}}} \simeq 10^{13} \left( \frac{1 \text{ g}}{M_{\text{BH}}} \right) \text{ GeV}. \quad (2)$$

Solving Eq. (1) leads to the time evolution of the PBH mass

$$M_{\text{BH}}(t) = M_{\text{in}} \left( 1 - \frac{t - t_{\text{in}}}{t_{\text{ev}}} \right)^{\frac{1}{3}}, \quad (3)$$

where  $t_{\text{in}}$  is the time at formation, and  $t_{\text{ev}}$  is the evaporation time, i.e.

$$t_{\text{ev}} = \Gamma_{\text{BH}}^{-1} = \frac{M_{\text{in}}^3}{3\epsilon M_P^4} \simeq 2.4 \times 10^{-28} \left( \frac{M_{\text{in}}}{1 \text{ g}} \right)^3 \text{ s}. \quad (4)$$

We see that PBHs with masses  $\lesssim 10^9$  g decay *before* the beginning of the nucleosynthesis process, and are not constrained by CMB data. On the other hand, the initial PBH mass  $M_{\text{in}}$  is bounded by the size of the horizon at the end of inflation,

$$M_{\text{in}} \gtrsim H_{\text{end}}^{-3} \rho_{\text{end}} \sim \frac{M_P^3}{\sqrt{\rho_{\text{end}}}} \simeq 1 \text{ g}. \quad (5)$$

Taking into account the above constraints, we restrict our analysis to the following PBH mass range:

$$1 \text{ g} \lesssim M_{\text{in}} \lesssim 10^9 \text{ g}. \quad (6)$$

However, this mass range drastically changes if one takes into account the memory burden effect, as we will see in a following section.

### B. PBH reheating

It was shown in [16, 28] that PBHs can reheat the Universe through their Hawking radiation, even in the presence of an inflaton field, whose oscillations dominate the energy budget of the Universe at the end of inflation. Obviously, if the PBHs lifetime is longer than the inflaton one, the PBH population dominates the reheating process. However, as it was shown in [16], this is not the only situation where the reheating is dominated by the PBHs. Indeed, as the inflaton energy density  $\rho_\phi \propto a^{-3(1+w_\phi)}$ , with an equation of state  $P_\phi = w_\phi \rho_\phi$ , for  $w_\phi > 0$ , there exists the possibility for the PBHs to dominate the energy budget even *before* the inflaton decay. This happens for a sufficient amount of PBH at formation time. Defining

$$\beta = \frac{\rho_{\text{BH}}(t_{\text{in}})}{\rho_{\text{tot}}(t_{\text{in}})} \simeq \frac{\rho_{\text{BH}}(t_{\text{in}})}{\rho_\phi(t_{\text{in}})}, \quad (7)$$

<sup>1</sup>Which can be more complex depending on the context [41–44]. Note that we neglected the accretion effect [45, 46].

it was shown in [16] that PBH energy density dominates over the inflaton energy density for  $\beta$  above a critical value

$$\beta_c = \left( \frac{\epsilon}{(1+w_\phi)2\pi\gamma} \right)^{\frac{2w_\phi}{1+w_\phi}} \left( \frac{M_P}{M_{\text{in}}} \right)^{\frac{4w_\phi}{1+w_\phi}}, \quad (8)$$

where  $\gamma$  is the collapse efficiency parameter, of the order  $\mathcal{O}(1)$ , defined by

$$M_{\text{in}} = \frac{4\pi\gamma M_P^2}{H_{\text{in}}}, \quad \gamma = w_\phi^{3/2}, \quad (9)$$

see appendix B, and especially Eq. (B8) for a details computation of  $\beta_c$ . This corresponds for instance to  $\beta_c \simeq 3 \times 10^{-6}$  for a quartic potential of the inflaton,  $V(\phi) \propto \phi^4$  ( $w_\phi = 1/3$ ), and  $M_{\text{in}} = M_{\text{min}} = 1$  g.

In the present work, we consider that the reheating is induced by the PBHs population. In other words, the successive phases are : inflation, inflaton oscillations, PBH domination, followed by a radiative Universe. In this case, the reheating temperature is obtained by solving

$$\rho_{\text{RH}} = \alpha T_{\text{RH}}^4 = 3M_P^2 H^2(T_{\text{RH}}) = \frac{4}{3} \frac{M_P^2}{t_{\text{ev}}^2} = 12\epsilon^2 \frac{M_P^{10}}{M_{\text{BH}}^6}, \quad (10)$$

which implies

$$T_{\text{RH}} = \left( \frac{12\epsilon^2}{\alpha} \right)^{\frac{1}{4}} \sqrt{\frac{M_P^5}{M_{\text{BH}}^3}} \simeq 3.5 \times 10^{10} \left( \frac{1 \text{ g}}{M_{\text{BH}}} \right)^{\frac{3}{2}} \text{ GeV}, \quad (11)$$

with  $\alpha = \frac{g_{\text{RH}}\pi^2}{30}$ ,  $g_{\text{RH}}$  being the relativistic degrees of freedom at  $T_{\text{RH}}$ . Note that, in the semi-classical approach, we can approximate  $M_{\text{BH}} \simeq M_{\text{in}}$  during the whole evaporation process. This will not be the case when we examine the possibility of a memory burden effect. Note that  $T_{\text{RH}}$  is different from the Hawking temperature  $T_{\text{BH}}$  in Eq. (2), even if they are related in some-way. The Hawking temperature represents the *efficiency* of the evaporation, whereas the reheating temperature represents the *lifetime* of the PBH, and is then naturally cooler.

### C. The burden effect

It was shown that in a system of high storage capacity, the information stored in the system tends to backreact to resist to the process of information lost [47, 48]. Applied to black holes, this corresponds to a modification of the semi-classical approach to their decay process [17–19]. Naively, this backreaction effects should become

efficient when the leftover information is of the magnitude of the information lost, or  $\Delta M_{\text{BH}} \sim M_{\text{BH}}$ . The authors of [49] even proposed that the burdening sequence is a continuous process, beginning at the onset of their formation. The aim of this section is to explain with simple arguments how the memory burden affects the phenomenology of PBH in the early Universe. For interested readers, we've devoted a complete section B in the appendix, where all our results are derived in detail.

When we take into account the memory burden effect, the evaporation of a PBH occurs in two phases. Initially, the PBH behaves in a semi-classical way, until a non-negligible fraction of lost information triggers a black hole back-reaction, effectively slowing down the evaporation process. To model the phenomenon, we suppose that the semi-classical regime is valid until the mass of the PBH reaches a certain value,  $M_{\text{BH}} = qM_{\text{in}}$ , with  $0 < q < 1$ . There are no real microscopic motivated values for  $q$ , but we can expect that when  $q \sim \frac{1}{2}$ , the amount of information lost is of the order of the amount of information still inside the PBH. At that stage, the back-reaction effect should be triggered, as a survival reflex of the PBH. This value of  $q$  is also the benchmark point used by the authors of [17, 19].

The same authors proposed to model the back-reaction effect, by a change in the semi-classical evaporation equation,

$$\left. \frac{dM_{\text{BH}}}{dt} \right|_{\text{burden}} = \frac{1}{S^n} \frac{dM_{\text{BH}}}{dt} = -2^n \epsilon \times \frac{M_P^{2n+4}}{M_{\text{BH}}^{2n+2}}, \quad (12)$$

where  $dM_{\text{BH}}/dt$  is given by Eq. (1) and  $n > 0$ . In Eq. (12),  $S$  is the PBH entropy

$$S = \frac{1}{2} \frac{M_{\text{BH}}^2}{M_P^2}. \quad (13)$$

Even if the dependence on  $S$  in Eq. (12) can be justified by analogy with the theory of information [47, 48, 50], we can also stay agnostic and suppose that the loss in the decay rate is an inverse function of the entropy, which can be modeled by a power law at the first order. The evolution of the PBH is then modified, and is obtained by integrating Eq. (12) :

$$M_{\text{BH}}(t) = qM_{\text{in}} [1 - \Gamma_{\text{BH}}^n(t - t_q)]^{\frac{1}{3+2n}}, \quad (14)$$

with

$$\Gamma_{\text{BH}}^n = 2^n(3+2n)\epsilon \times M_P \left( \frac{M_P}{qM_{\text{in}}} \right)^{3+2n}. \quad (15)$$

and

$$t_q = \frac{1 - q^3}{\Gamma_{\text{BH}}^0}, \quad (16)$$

is the time which ends the semi-classical phase. Note that for  $n = 0$  and  $q = 1$ , we recover the semiclassical PBH lifetime  $(\Gamma_{\text{BH}})^{-1} = \frac{M_{\text{in}}^3}{3\epsilon M_P^4}$ .

The reheating temperature obtained in Eq. (11) then becomes

$$\alpha T_{\text{RH}}^4 = \frac{4}{3} M_P^2 (\Gamma_{\text{BH}}^n)^2 = \frac{4 \times 2^{2n} (3 + 2n)^2}{3q^{6+4n}} \epsilon^2 \frac{M_P^{10+4n}}{M_{\text{in}}^{6+4n}}$$

$$\Rightarrow T_{\text{RH}}|_{n=1}^{q=\frac{1}{2}} \simeq 1.6 \times 10^6 \left( \frac{1 \text{ g}}{M_{\text{in}}} \right)^{\frac{5}{2}} \text{ GeV}, \quad (17)$$

which is lower than the reheating temperature *without* burdening, as expected because of a longer PBH lifetime. Other constraints on the burden parameters can be inferred from BBN bounds [51], WIMP/FIMP production modes [52], or observations of galactic and extra-galactic sources [53–57] and lepto/baryogenesis [58, 59].

### III. PRIMORDIAL GRAVITATIONAL WAVE

It is well known that quantum fluctuations are sources of gravitational waves during inflation [60]. These stochastic gravitational waves are called *primordial* gravitational waves (PGW). Because the gravitons do not thermalize, PGWs are a unique opportunity to test the physics of reheating. Given the energy density involved during inflation, the spectrum of gravitational waves produced covers a very large range of frequencies. For instance, at the end of inflation, the energy available under the form of oscillations of the inflaton, is of the order of  $\sim m_\phi$ . It would generate waves of frequency

$$f_{\text{end}} \sim \left( \frac{m_\phi}{4 \times 10^{13} \text{ GeV}} \right) 10^{37} \text{ Hz}, \quad (18)$$

which redshifts as  $a_{\text{end}}/a_0$  nowadays. The redshift is obviously highly dependent on the species which dominate the expansion rate  $H$ , and the reheating process. However, in a radiation-like Universe, which happens in the case of an instant reheating, or a Universe dominated by the oscillations of an inflaton with a quartic potential, we have  $a_{\text{end}}/a_0 \sim T_0/\rho_{\text{end}}^{\frac{1}{4}} \sim 10^{-29}$ , where we took  $\rho_{\text{end}} \sim 10^{64} \text{ GeV}^4$ , or

$$f_0^{\text{end}} \sim m_\phi \frac{a_{\text{end}}}{a_0} \sim \left( \frac{m_\phi}{4 \times 10^{13} \text{ GeV}} \right) 10^8 \text{ Hz}. \quad (19)$$

This frequency corresponds roughly to the end of the PGW spectrum, region  $A_3/C$  in Fig. 1. In the following, we will describe the energy spectrum from the lower frequencies (region  $A_1$  of Fig. 1, corresponding to the modes entering in the horizon during the radiation dominated era) to the higher ones (region  $A_3$ , corresponding to the modes entering at the very end of inflation).

#### A. The radiation dominated era ( $A_1$ )

The density of energy stored under the form of GW of mode  $k$  can be estimated by [61, 62]

$$\rho_{\text{GW}} \equiv \frac{d\rho_{\text{GW}}(k)}{d \log k} \sim k^2 \langle h_{ij} h_{ij} \rangle, \quad (20)$$

where

$$\langle h_{ij} h_{ij} \rangle \sim \left( \frac{H_{\text{end}}}{2\pi} \right)^2, \quad (21)$$

are the tensor fluctuations produced during inflation. The expression (20) can be understood noting that the solution of the equation of motion for modes  $h_{ij}$  staying below the horizon during the whole inflation ( $k \ll H_{\text{end}}$ ) behaves as [63]

$$h_{ij} \sim \frac{H_{\text{end}}}{\sqrt{2} k^{\frac{3}{2}}} e^{ikt}, \quad (22)$$

which implies

$$d\rho_{\text{GW}} \sim \frac{k^3}{2\pi^2} \nabla |h_{ij}|^2 d \ln k \sim k^2 \left( \frac{H_{\text{end}}}{2\pi} \right)^2 d \ln k. \quad (23)$$

For interested readers, we develop in appendix A, especially Eq. (A4), the details of the calculation which lead to the exact PGW spectrum that we used for our numerical analysis. However, the expression (20) remains a good approximation for understanding the mechanism, and the final shape of the spectrum that we explain in detail in appendix A.

After the end of inflation, the wave mode  $k < H_{\text{end}}$  reenters inside the horizon when  $k \sim H$ , with a frequency  $f = k/2\pi$ . Once produced, the energy density  $\rho_{\text{GW}}$  evolves in the same way as the radiation density  $\rho_R$ , i.e  $\rho_{\text{GW}} \propto a^{-4}$ . The ratio  $\rho_{\text{GW}}/\rho_R$  is then constant (up to decoupled degrees of freedom) and is given by

$$\frac{\rho_{\text{GW}}}{\rho_R}(a) = \frac{k^2 H_{\text{end}}^2}{4\pi^2 \rho_R} \sim \frac{1}{12\pi^2} \frac{H_{\text{end}}^2}{M_P^2} \simeq 5.3 \times 10^{-14}, \quad (24)$$

where we used the fact that the Universe is dominated by  $\rho_R = 3M_P^2 H^2$  after the reheating phase, and  $H = k$  at horizon re-entry. In Eq. (24), we took  $H_{\text{end}} = 2.5 \times 10^{-6} M_P$ , which will be our benchmark point throughout our present study. The spectrum is flat, as expected.

The relic abundance  $\Omega_{\text{GW}} h^2$  is then

$$\Omega_{\text{GW}} h^2 = \frac{\rho_{\text{GW}}}{\rho_{\text{tot}}} h^2 = \frac{\rho_{\text{GW}}}{\rho_R} \Omega_R h^2 \simeq 4.1 \times 10^{-5} \frac{\rho_{\text{GW}}}{\rho_R}, \quad (25)$$

where we neglected the change in the relativistic degrees of freedom between the horizon crossing and present time.

Combining with Eq. (24), we obtain

$$\Omega_{GW}^{A_1} h^2 \simeq \frac{4.1 \times 10^{-5}}{12\pi^2} \left( \frac{H_{\text{end}}}{M_P} \right)^2 \simeq 2.2 \times 10^{-18}, \quad (26)$$

which is effectively what we observe in the region  $A_1$  of Fig. 1, where the decoupling of the degrees of freedom has been taken into account.

This region  $A_1$  corresponds to the gravitational waves produced *after* reheating. We clearly recognize the scale-invariant form of the spectrum, whose frequencies span from the lower ones, the ones entered in the horizon at late time, to the highest one, the ones entered in the horizon at the reheating time<sup>2</sup>  $a_{\text{RH}}$ . The form of the spectrum then changes for higher frequencies, region  $A_2$ . This is because before  $a_{\text{RH}}$ , the evolution of the Universe is drastically different. It is dominated by the PBH which behaves like dust, and not radiation. We therefore expect the spectrum break to appear at a frequency  $f_0^{\text{RH}}$  corresponding to the end of reheating, or

$$f_0^{\text{RH}} = \frac{k_{\text{RH}}}{2\pi} \frac{a_{\text{RH}}}{a_0} = \sqrt{\frac{\alpha}{3}} \frac{T_{\text{RH}}^2}{2\pi M_P} \left( \frac{g_0}{g_{\text{RH}}} \right)^{\frac{1}{3}} \frac{T_0}{T_{\text{RH}}} \quad (27)$$

which gives

$$f_0^{\text{RH}} = g_0^{\frac{1}{3}} g_{\text{RH}}^{\frac{1}{6}} \frac{T_0 T_{\text{RH}}}{6\sqrt{10} M_P} \simeq 946 \left( \frac{1 \text{ g}}{M_{\text{BH}}} \right)^{\frac{3}{2}} \text{ Hz}, \quad (28)$$

where in the last expression, we used Eq. (11). This frequency of transition PBH domination  $\rightarrow$  radiation domination is indeed the one we observe in Fig. 1.

### B. The PBH domination era ( $A_2$ )

For frequencies  $f^0$  larger than  $f_{\text{RH}}^0$ , the PGW modes entered in the horizon during the phase of PBH domination. The evolution of the Hubble rate (and thus the horizon of re-entry) is then not governed by a radiation field, but by a dust, following  $H(a) \propto a^{-\frac{3}{2}}$ . Using Eq. (20), the present GW energy density is then

$$\begin{aligned} \rho_{\text{GW}}(a_{\text{RH}}) &= \rho_{\text{GW}}(a_{\text{hc}}) \left( \frac{a_{\text{hc}}}{a_{\text{RH}}} \right)^4 = \frac{H_{\text{end}}^2}{4\pi^2} k_{\text{hc}}^2 \left( \frac{a_{\text{hc}}}{a_{\text{RH}}} \right)^4 \\ &= \frac{H_{\text{end}}^2}{4\pi^2} k_{\text{RH}}^2 \left( \frac{a_{\text{hc}}}{a_{\text{RH}}} \right)^2 \\ \Rightarrow \frac{\rho_{\text{GW}}(a_{\text{RH}})}{\rho_R(a_{\text{RH}})} &= \frac{1}{36\pi^2} \frac{H_{\text{end}}^2}{M_P^2} \frac{\rho_{\text{RH}}}{M_P^2 k_{\text{RH}}^2}, \end{aligned} \quad (29)$$

where  $a_{\text{hc}}$  is the scale factor at horizon crossing,  $k_{\text{hc}} = H(a_{\text{hc}})$ , and

$$3M_P^2 k_{\text{hc}}^2 = \rho(a_{\text{hc}}) = \rho_{\text{RH}} \left( \frac{a_{\text{RH}}}{a_{\text{hc}}} \right)^3 \Rightarrow \frac{a_{\text{hc}}}{a_{\text{RH}}} = \frac{\rho_{\text{RH}}}{3M_P^2 k_{\text{RH}}^2}.$$

where we used  $\rho(a_k) = 3M_P^2 k^2$  at the horizon entry of the mode  $k$ . From  $\rho_{\text{RH}}$  given by Eq. (10), we deduce, neglecting the change in number of degrees of freedom (see the appendix A and Eq. (A4) for a detailed calculation),

$$\frac{\rho_{\text{GW}}(a_0)}{\rho_R(a_0)} \simeq \frac{\rho_{\text{GW}}(a_{\text{RH}})}{\rho_R(a_{\text{RH}})} \simeq \frac{1}{36\pi^2} \frac{H_{\text{end}}^2}{M_P^2} \frac{\alpha T_{\text{RH}}^2 T_0^2}{M_P^2 k_0^2}, \quad (30)$$

which implies

$$\begin{aligned} \Omega_{GW}^{A_2} h^2 &\simeq \frac{4.1 \times 10^{-5} \alpha}{36\pi^2} \left( \frac{H_{\text{end}} T_{\text{RH}}}{M_P^2} \right)^2 \left( \frac{T_0}{2\pi f_0} \right)^2 \\ &\simeq 2.3 \times 10^{-19} \left( \frac{T_{\text{RH}}}{10^{10} \text{ GeV}} \right)^2 \left( \frac{10^3 \text{ Hz}}{f_0} \right)^2, \end{aligned} \quad (31)$$

where we used Eq. (25), and which is effectively what we observe in Fig. 1. Replacing  $T_{\text{RH}}$  by its expression as function of  $M_{\text{BH}}$ , Eq. (11), we then obtain in the semi-classical approximation

$$\begin{aligned} \Omega_{GW}^{A_2} h^2 &\simeq \frac{4.1 \times 10^{-5} \epsilon \sqrt{3\alpha}}{18\pi^2} \left( \frac{H_{\text{end}}^2 M_P}{M_{\text{BH}}^3} \right) \left( \frac{T_0}{2\pi f_0} \right)^2 \\ &\simeq 2.8 \times 10^{-18} \left( \frac{1 \text{ g}}{M_{\text{BH}}} \right)^3 \left( \frac{10^3 \text{ Hz}}{f_0} \right)^2. \end{aligned} \quad (32)$$

### C. The inflaton domination era ( $A_3$ )

The shape of the PGW spectrum described above is valid throughout the period of PBH domination, which begins at a scale factor  $a_{\text{BH}}$  defined by

<sup>2</sup>Throughout this work, we will use the notion of ‘time’ (before, after) indiscriminately with the notion of scale factor.



$$\rho_{\text{BH}}(a_{\text{BH}}) = \rho_{\phi}(a_{\text{BH}}). \quad (33)$$

To express this condition as function of  $M_{\text{BH}}$ , one needs to introduce a new parameter,  $\beta$ , which is the ratio between the energy density stored under the form of PBH and the total (inflaton) energy density at the time of PBH formation  $a_{\text{in}}$ ,

$$\beta = \frac{\rho_{\text{BH}}(a_{\text{in}})}{\rho_{\phi}(a_{\text{in}})}. \quad (34)$$

Combining Eqs. (33) and (34) with  $\rho_{\phi}(a_{\text{BH}}) = \rho_{\phi}(a_{\text{in}}) \left(\frac{a_{\text{in}}}{a_{\text{BH}}}\right)^{3(1+w_{\phi})}$  and  $\rho_{\text{BH}}(a_{\text{BH}}) = \rho_{\text{BH}}(a_{\text{in}}) \left(\frac{a_{\text{in}}}{a_{\text{BH}}}\right)^3$ , we found

$$\frac{a_{\text{in}}}{a_{\text{BH}}} = \beta^{\frac{1}{3w_{\phi}}}. \quad (35)$$

The size of the horizon at  $a_{\text{BH}}$ , which defines the highest frequency of the PBH domination era is then

$$H(a_{\text{BH}}) = H(a_{\text{in}}) \left(\frac{a_{\text{in}}}{a_{\text{BH}}}\right)^{\frac{3(1+w_{\phi})}{2}} = 4\pi \frac{M_P^2}{M_{\text{BH}}} \beta^{\frac{1+w_{\phi}}{2w_{\phi}}}, \quad (36)$$

where we used the approximation that all the mass inside the horizon collapses into PBH at  $a_{\text{in}}$ , or<sup>3</sup>

$$M_{\text{BH}} \sim M_{\text{in}} = \frac{4}{3}\pi H^{-3}(a_{\text{in}})\rho_{\phi}(a_{\text{in}}) = 4\pi \frac{M_P^2}{H(a_{\text{in}})}. \quad (37)$$

The present frequency corresponding to  $k_{\text{BH}} = H(a_{\text{BH}})$  is then

$$\begin{aligned} f_0^{\text{BH}} &= \frac{k_{\text{BH}} a_{\text{BH}} a_{\text{RH}}}{2\pi a_{\text{RH}} a_0} = \frac{1}{2\pi 3^{\frac{1}{3}}} \frac{H^{\frac{1}{3}}(a_{\text{BH}}) \rho_{\text{RH}}^{\frac{1}{3}}}{M_P^{\frac{2}{3}}} \frac{T_0}{T_{\text{RH}}} \frac{g_0^{\frac{1}{3}}}{g_{\text{RH}}^{\frac{1}{3}}} \\ &= \frac{1}{2\pi} \left(\frac{4\pi}{3}\right)^{\frac{1}{3}} \frac{\rho_{\text{RH}}^{\frac{1}{3}}}{M_{\text{BH}}^{\frac{1}{3}}} \beta^{\frac{1+w_{\phi}}{6w_{\phi}}} \frac{T_0}{T_{\text{RH}}} \frac{g_0^{\frac{1}{3}}}{g_{\text{RH}}^{\frac{1}{3}}} \\ &\simeq 2.6 \times 10^6 \left(\frac{T_{\text{RH}}}{10^{10} \text{ GeV}}\right)^{\frac{1}{3}} \left(\frac{1 \text{ g}}{M_{\text{BH}}}\right)^{\frac{1}{3}} \beta^{\frac{1+w_{\phi}}{6w_{\phi}}} \text{ Hz}, \end{aligned} \quad (38)$$

where we used

$$\frac{a_{\text{BH}}}{a_{\text{RH}}} = \left(\frac{\rho_{\text{RH}}}{\rho(a_{\text{BH}})}\right)^{\frac{1}{3}} = \frac{\rho_{\text{RH}}^{\frac{1}{3}}}{(3M_P^2 H^2(a_{\text{BH}}))^{\frac{1}{3}}}. \quad (39)$$

Replacing the expression (11) for  $T_{\text{RH}}$ , and taking  $w_{\phi} = \frac{1}{2}$ , we find

$$f_0^{\text{BH}} \simeq 1.2 \times 10^4 \left(\frac{1 \text{ g}}{M_{\text{BH}}}\right)^{\frac{5}{6}} \sqrt{\frac{\beta}{10^{-5}}} \text{ Hz}, \quad (40)$$

which is effectively the inflection point of the transition PBH-domination  $\rightarrow$  inflaton-domination ( $A_2 \rightarrow A_3$ ) in Fig. 1. The GW density at this frequency is then given by Eq.(31) with  $f_0 = f_0^{\text{BH}}$ , or

$$\Omega_{\text{GW}} h^2(f_0^{\text{BH}}) \simeq 3.9 \times 10^{-20} \left(\frac{10^{-5}}{\beta}\right) \left(\frac{1 \text{ g}}{M_{\text{BH}}}\right)^{\frac{4}{3}}. \quad (41)$$

For larger frequencies,  $f_0 > f_0^{\text{BH}}$ , the PGW propagates in a medium dominated by the inflaton field, whose equation of state is  $p_{\phi} = w_{\phi} \rho_{\phi}$ . Knowing the value of  $\Omega_{\text{GW}}$  at  $f_0^{\text{BH}}$ , one then needs to just know the behavior  $\Omega_{\text{GW}} = f(f_0)$  in the generic case of a background dominated by a field with an equation of state  $w_{\phi}$ . From

$$\Omega_{\text{GW}}(a_{\text{hc}}) \sim \frac{H_{\text{end}}^2}{12\pi^2 M_P^2} \frac{k_{\text{hc}}^2}{H^2(a_{\text{hc}})} \sim \frac{H_{\text{end}}^2}{12\pi^2 M_P^2}, \quad (42)$$

we deduce

$$\begin{aligned} \Omega_{\text{GW}}(a_{\text{BH}}) &= \frac{H_{\text{end}}^2}{12\pi^2 M_P^2} \frac{(a_{\text{hc}}/a_{\text{BH}})^4}{(a_{\text{hc}}/a_{\text{BH}})^{3(1+w_{\phi})}} \\ &= \frac{H_{\text{end}}^2}{12\pi^2 M_P^2} \left(\frac{\rho_{\text{BH}}}{3M_P^2}\right)^{\frac{1-3w_{\phi}}{1+3w_{\phi}}} k_{\text{BH}}^{\frac{6w_{\phi}-2}{3w_{\phi}+1}}, \end{aligned} \quad (43)$$

where we used the fact that  $H$  redshifts as  $H(a) \propto a^{-3(1+w_{\phi})}$ ,  $\rho_{\text{GW}} \propto a^{-4}$  after horizon crossing, and

$$\begin{aligned} \left(\frac{a_{\text{BH}}}{a_{\text{hc}}}\right)^{3(1+w_{\phi})} &= \frac{3M_P^2 H^2(a_{\text{hc}})}{\rho_{\text{BH}}} = \frac{3M_P^2 k_{\text{BH}}^2 (a_{\text{BH}}/a_{\text{hc}})^2}{\rho_{\text{BH}}} \\ \Rightarrow \frac{a_{\text{BH}}}{a_{\text{hc}}} &= \left(\frac{3M_P^2 k_{\text{BH}}^2}{\rho_{\text{BH}}}\right)^{\frac{1}{1+3w_{\phi}}}. \end{aligned} \quad (44)$$

Note that Eq. (43) recovers the behavior  $\Omega_{\text{GW}} = \text{cst}$  in the radiation dominated Universe ( $w_{\phi} = \frac{1}{3}$ ), see Eq. (26) and  $\Omega_{\text{GW}} \propto k^{-2}$  for matter dominated ( $w_{\phi} = 0$ ) case, see Eq. (31). For  $w_{\phi} = \frac{1}{2}$ , corresponding to an inflaton potential after inflation  $V(\phi) \propto \phi^6$ , we obtain  $\Omega_{\text{GW}} \sim k^{\frac{2}{5}}$ , which corresponds indeed to what we observe in Fig. 1, in the region  $A_3$ . Combining Eq. (43) with Eqs. (40) and (41), we obtain for  $w_{\phi} = \frac{1}{2}$ ,

$$\Omega_{\text{GW}}^{A_3} h^2 \simeq 10^{-19} \left(\frac{1 \text{ g}}{M_{\text{BH}}}\right) \left(\frac{10^{-5}}{\beta}\right)^{\frac{4}{5}} \left(\frac{f_0}{10^5 \text{ Hz}}\right)^{\frac{2}{5}}. \quad (45)$$

<sup>3</sup>The exact expression depends on the efficiency of the collapse defined by a parameter  $\gamma$  which is function of  $w_{\phi}$  and described in the appendix.

As a conclusion, we analyzed in this section the features of a PGW spectrum in a Universe passing successively from an inflaton era, PBH era and radiation dominated era. Our results are summarized by the Eqs. (26), (31) and (45) in the semiclassical approximation. As we mentioned earlier, one needs to keep in mind that, despite the challenges of observations [64–66], a measure of PGW spectrum is a direct and clear insight on the history of pre-BBN physics.

#### D. Burdening the spectrum

The memory burden effect affects the shape of the PGW spectrum with several respects, as one can see in Fig. 1. Firstly, the lifetime of the PBHs being longer, the reheating occurs at lower frequencies (smaller Hubble rate). That pushes the transition  $\Omega_{GW}h^2 \propto f_0^{-2} \rightarrow \Omega_{GW}h^2 \sim 10^{-18}$  from  $f_0^{RH}$  in Eq. (28) to

$$f_0^{RH}|_n^q = \frac{\alpha^{\frac{1}{4}} \sqrt{\epsilon} 2^{\frac{n+1}{2}}}{3^{\frac{3}{4}} 2\pi} \sqrt{3+2n} \left( \frac{M_P}{q M_{BH}} \right)^{\frac{3}{2}+n} \left( \frac{g_0}{g_{RH}} \right)^{\frac{1}{3}} T_0, \quad (46)$$

where we used Eq. (17) for  $T_{RH}$ . Note that we recover the expression (28) for  $n = 0$  and  $q = 1$ . In our benchmark case ( $n = 1$ ,  $q = \frac{1}{2}$ ), this gives

$$f_0^{RH}|_{n=1}^{q=\frac{1}{2}} = \frac{2^{\frac{7}{2}} \sqrt{5\epsilon}}{3^{\frac{3}{4}} 2\pi} \alpha^{\frac{1}{4}} \left( \frac{g_0}{g_{RH}} \right)^{\frac{1}{3}} \left( \frac{M_P}{M_{BH}} \right)^{\frac{5}{2}} T_0 \\ \simeq 1.1 \times 10^{-1} \left( \frac{1 \text{ g}}{M_{BH}} \right)^{\frac{5}{2}} \text{ Hz}, \quad (47)$$

which is clearly what we see in Fig. 1.

The memory burden also affects the present frequency at which the PBHs begin to dominate the Universe. Indeed, while the formation time remains the same, the longer matter domination era induced by the burdening affects the redshift of the corresponding PGW frequencies. Combining Eq. (38) with Eq. (17), we obtain

$$f_0^{BH}|_n^q = \frac{\alpha^{\frac{1}{4}} (3+2n)^{\frac{1}{6}} 2^{\frac{n-1}{6}} \epsilon^{\frac{1}{6}} \beta^{\frac{1+w_\phi}{6w_\phi}}}{3^{\frac{5}{12}} \pi^{\frac{2}{3}} q^{\frac{1}{2}+\frac{n}{3}}} \\ \times \left( \frac{M_P}{M_{BH}} \right)^{\frac{5}{6}+\frac{n}{3}} \left( \frac{g_0}{g_{RH}} \right)^{\frac{1}{3}} T_0, \quad (48)$$

which gives, for  $q = \frac{1}{2}$  and  $n = 1$

$$f_0^{BH}|_{n=1}^{q=\frac{1}{2}} \simeq 14 \left( \frac{1 \text{ g}}{M_{BH}} \right)^{\frac{7}{6}} \sqrt{\frac{\beta}{10^{-8}}} \text{ Hz}, \quad (49)$$

which is also what we see in Fig. 1, where we took  $\beta = 10^{-8}$ .

The behavior of  $\Omega_{GW}h^2$  between  $f_0^{BH}$  and  $f_0^{RH}$  is the same with or without the burden case, as in both cases, the Universe is dominated by PBH and is affected by the same redshift, which is also what we see in Fig. 1.

As a conclusion, we see that the memory burden affects the PGW, acting as a heavier PBH concerning the reheating temperature (because increasing the PBH lifetime), and thus pushing  $f_0^{RH}$  toward lower values (compare Eq. (47) with Eq. (28)), but still formed at early time because the burdening *does not* affect the formation and thus the domination time,  $a_{BH}$ . As a consequence, the memory burden spectrum of PGW is enlarged towards *lower* frequencies. The gap between  $f_0^{RH}$  and  $f_0^{BH}$  could then be a clear signature of the presence of a burdening effect in the early Universe.

### IV. INFLATON SCATTERING

#### A. Generalities

Another source of graviton involves the inflaton scattering through the exchange of a graviton, see for instance Fig. 2 [67]. This production of graviton can be interpreted as the high frequency counterpart of fluctuations, that never left the horizon during inflation [63]. It was shown recently in [68], and more generically in [62] that this Feynman calculation is equivalent to a Bogoliubov approach for modes  $k \gg k(a_{\text{end}}) = k_{\text{end}}$ .

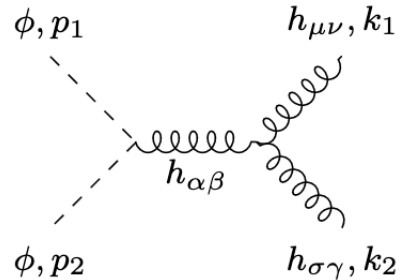


Figure 2. Example of a gravitational process contributing to the gravitational wave background through inflaton scattering.

This production mode depends strongly on the equation of state before reheating, through the dilution of the modes  $\omega_\phi(a)$  of the inflaton field. Indeed, whereas for a quadratic potential,  $\omega_\phi = \text{cte} = m_\phi$ , for a quartic potential,  $\omega_\phi(a) \sim \omega_{\text{end}} \left( \frac{a_{\text{end}}}{a} \right)$ . For a potential  $V(\phi) \propto \phi^k$  during reheating,  $\omega_\phi(a) \propto \partial_\phi^2 V(\phi) \propto a^{-3\frac{k-2}{k+2}}$  [69–71]. It is important to note that the process pictured in Fig. 2 is not, *stricto-sensu*, a *scattering* but a transfer of energy from the oscillations of a *classical* background field

$\phi$  toward quantum fields, under the form of gravitons in our case. For a generic potential  $\phi^k$ , the exact computation necessitates a sum over a number of modes  $\omega_\phi^n(a), n = 1 \dots \infty$  [72–75]. The calculation can be tedious, and we describe the method in more detail in the appendix C. This precise calculation with a sum over the modes is the one we used for our numerical analysis.

However, it was also shown in [73] that treating the process as a scattering process gives (up to some numerical factors of the order of unity due to the symmetry factors and sum over the modes) a good approximation. It was also the method used in [63]. This is the approach we will use in this section to help the reader to understand the shape of the spectrum, the exact result being left in the appendix C.

### B. The Boltzmann equation

To compute the energy spectrum generated by the scattering of the inflaton, one needs to solve the Boltzmann equation

$$\frac{d\rho_{GW}}{dt} + 4H\rho_{GW} = 2 \times n_\phi^2 \times \sigma v \times \omega_\phi = \frac{\rho_\phi^2}{4\pi M_P^4} \omega_\phi, \quad (50)$$

where the factor 2 corresponds to 2 gravitons produced per scattering, and we used for the amplitude of the process<sup>4</sup>

$$|\mathcal{M}_{\phi\phi \rightarrow hh}|^2 \sim \frac{\omega_\phi^4}{M_P^4} \Rightarrow \sigma v \sim \frac{|\mathcal{M}_{\phi\phi \rightarrow hh}|^2}{8\pi\omega_\phi^2} \sim \frac{\omega_\phi^2}{8\pi M_P^4},$$

and

$$n_\phi^2 \times \sigma v \sim \left(\frac{\rho_\phi}{\omega_\phi}\right)^2 \times \frac{\omega_\phi^2}{8\pi M_P^4} \sim \frac{\rho_\phi^2}{8\pi M_P^4}. \quad (51)$$

To solve Eq. (50), we use the classical change of variable  $\frac{d}{dt} \rightarrow H a \frac{d}{da}$ , which gives

$$\frac{da^4 \rho_{GW}}{da} = \frac{a^3 \rho_\phi^2 \omega_\phi(a)}{4\pi H(a) M_P^4}. \quad (52)$$

Instead of integrating Eq. (52), we can use it to extract the spectrum of graviton as function of the present frequency  $f_0$ .

### C. The spectrum (C)

To obtain the relative spectrum as function of  $f_0$ , we use

$$f_0 = \frac{\omega_\phi(a)}{2\pi} \frac{a}{a_0} = \frac{\omega_{\text{end}}}{2\pi} \left(\frac{a_{\text{end}}}{a}\right)^{\frac{3}{k+2}} \frac{a}{a_0} \quad (53)$$

$$\Rightarrow d \ln f_0 = \frac{df_0}{f_0} = \left| \frac{8-2k}{k+2} \right| \frac{da}{a}, \quad (54)$$

which implies

$$\frac{d\rho_{GW}^0}{d \ln f_0} = \frac{1}{a_0^4} \frac{da^4 \rho_{GW}^0}{d \ln f_0} = \frac{1}{a_0^4} \frac{da^4 \rho_{GW}(a)}{d \ln f_0} \quad (55)$$

or, for a potential  $V(\phi) \sim \phi^k$ ,

$$\frac{d\rho_{GW}^0}{d \ln f_0} = \frac{1}{4\pi} \left| \frac{k+2}{8-2k} \right| \left( \frac{a}{a_0} \right)^4 \frac{\rho_\phi^2 \omega_\phi(a)}{H(a) M_P^4}, \quad (56)$$

where we used the fact that  $a^4 \rho_{GW}(a)$  is constant, and Eq. (52) combined with Eq. (54).

During the domination of the inflaton oscillations, we can write  $H(a) = \frac{\sqrt{\rho_\phi}}{\sqrt{3}M_P}$ . Using Eq. (53) we deduce that

$$\frac{a_{\text{end}}}{a} = \left( \frac{2\pi f_0}{\omega_{\text{end}}} \right)^{\frac{k+2}{2k-8}} \left( \frac{a_0}{a_{\text{end}}} \right)^{\frac{k+2}{2k-8}}. \quad (57)$$

Implementing the expression (57) into (56), with  $\rho_\phi(a) = \rho_{\text{end}} \left( \frac{a_{\text{end}}}{a} \right)^{\frac{6k}{k+2}}$ , we obtain

$$\frac{d\rho_{GW}^0}{d \ln f_0} = \left| \frac{k+2}{8-2k} \right| \frac{9H_{\text{end}}^3 \omega_{\text{end}}}{4\pi} \left( \frac{a_{\text{end}}}{a_0} \right)^{-\frac{9}{k-4}} \left( \frac{2\pi f_0}{\omega_{\text{end}}} \right)^{\frac{4k-7}{k-4}}. \quad (58)$$

For a quadratic potential, we obtain  $\frac{d\rho_{GW}^0}{d \ln f_0} \propto f_0^{-\frac{1}{2}}$ , whereas it is a monochromatic spectrum for a quartic potential<sup>5</sup>. In the case of our benchmark point,  $k = 6$ , we have

$$\frac{d\rho_{GW}^0}{d \ln f_0} = 9 \times (2\pi)^{\frac{15}{2}} H_{\text{end}}^3 \omega_{\text{end}} \left( \frac{a_0}{a_{\text{end}}} \right)^{\frac{9}{2}} \left( \frac{f_0}{\omega_{\text{end}}} \right)^{\frac{17}{2}}, \quad (59)$$

or,

$$\Omega_{GW}^C h^2 = \frac{h^2}{\rho_c} \frac{d\rho_{GW}^0}{d \ln f_0} \simeq 4.2 \times 10^{-18} \left( \frac{f_0}{4 \times 10^7 \text{ Hz}} \right)^{\frac{17}{2}}, \quad (60)$$

<sup>4</sup>In this calculation, we neglected the symmetry factors to simplify the reasoning. For the interested reader, the exact calculation is given in appendix C.

<sup>5</sup>In fact a sum of monochroms over all the inflaton modes.



where we took for the present critical density  $\rho_c = 8 \times 10^{47} h^2 \text{ GeV}^4$ ,  $H_{\text{end}} = 2 \times 10^{12} \text{ GeV}$ ,  $\omega_\phi = 4 \times 10^{13} \text{ GeV}$  and  $\frac{a_0}{a_{\text{end}}} = 10^{30}$ . This is effectively what we observe in Fig. (1), the highest frequency of the spectrum being given by  $f_{\text{end}}$  in Eq. (19).

## V. SCALAR FLUCTUATIONS

### A. Generalities

PBHs themselves can be a source of gravitational waves. Once dominating the Universe, their random distribution generates density fluctuations with a Poisson distribution since the locations of black holes are uncorrelated [76, 77]. The density (isocurvature) fluctuations of PBH,  $\delta\rho_{\text{BH}}$ , generates then potential (curvature) fluctuations  $\Phi$  through the Poisson equation

$$\nabla^2 \Phi \sim \frac{\delta\rho_{\text{BH}}}{M_P^2}. \quad (61)$$

After developing  $\Phi$  in its Fourier modes  $\Phi_k$ , Eq. (61) gives

$$\Phi_k \sim -\frac{k_{\text{BH}}^2}{k^2} \frac{\delta\rho_{\text{BH}}}{\rho_{\text{BH}}}, \quad (62)$$

where  $k_{\text{BH}} = H(a_{\text{BH}})$  is the horizon size at the onset of PBHs domination. A more precise solution of the Einstein's equation for the gravitational potential, taking into account long wavelength modes, gives [76]

$$\Phi_k \simeq -\left(5 + \frac{4}{9} \frac{k^2}{k_{\text{BH}}^2}\right)^{-1} \frac{\delta\rho_{\text{BH}}}{\rho_{\text{BH}}}. \quad (63)$$

Then, the scalar fluctuations  $\Phi$  source tensor perturbations  $h_{ij}$  of the metric

$$ds^2 = (1 - 2\Phi)dt^2 - a^2(t) \left[ \delta_{ij}(1 + 2\Phi) + \frac{2}{M_P} h_{ij} \right] dx^i dx^j, \quad (64)$$

under the form of gravitational waves which follows the equation of motion

$$h''_{k,\lambda} + 2\mathcal{H}h'_{k,\lambda} + k^2 h_{k,\lambda} = \mathcal{S}_{k,\lambda}, \quad (65)$$

where the derivatives are with respect to the conformal time  $\tau$ ,  $dt = a(\tau)d\tau$  and the source function  $\mathcal{S}_{k,\lambda}$  is given in appendix D, Eq. (D3). For the interested reader, we also describe in the appendix how we obtain the power spectra from the equation of motion (65). We discuss in particular the issue of the cutoff scales. In the core of this paper, we want to describe the main features of the spectrum, using if necessary rough approximations, such that the reader can understand the behavior of the GW generated by density perturbations, which corresponds to the regions  $B_i$  of Fig. 1.

### B. The spectrum ( $B_1$ and $B_2$ )

While we explain in more details how we obtained the spectrum  $B_1$  in Appendix D, we want in this section to help the reader to understand its main shape. Supposing an almost instantaneous PBH decay, it is easy to understand that the higher frequency,  $f_{UV}$  corresponds roughly to the mean inverse distance  $d_{\text{BH}}$  between two PBHs, or

$$\begin{aligned} f_{UV}(a_{\text{ev}}) &\sim \frac{1}{2\pi d_{\text{BH}}} \frac{a_{\text{in}}}{a_{\text{ev}}} = \frac{1}{2\pi} \left( \frac{4\pi}{3} n_{\text{BH}}(a_{\text{in}}) \right)^{\frac{1}{3}} \frac{a_{\text{in}}}{a_{\text{ev}}} \\ &= \frac{1}{2\pi} \left( \frac{4\pi}{3} n_{\text{BH}}(a_{\text{ev}}) \right)^{\frac{1}{3}} = \frac{2^{\frac{1}{3}}}{(3\pi)^{\frac{2}{3}}} \left( \frac{M_P^2 \Gamma_{\text{BH}}^2}{M_{\text{BH}}} \right)^{\frac{1}{3}}, \end{aligned} \quad (66)$$

where we used  $n_{\text{BH}}(a_{\text{ev}}) = \frac{\rho_{\text{RH}}}{M_{\text{BH}}}$ , with

$$\rho_{\text{RH}} = 3M_P^2 H^2(a_{\text{ev}}) = \frac{4}{3} M_P^2 \Gamma_{\text{BH}}^2. \quad (67)$$

After redshifting  $f_{UV}$  from  $a_{\text{RH}} (\equiv a_{\text{ev}})$  to  $a_0$ , we obtain in, the semiclassical approximation, with  $\Gamma_{\text{BH}}$  given by Eq. (4), and  $T_{\text{RH}}$  by Eq. (11) :

$$f_0^{UV} = \left( \frac{g_0}{g_{\text{RH}} \pi^2} \right)^{\frac{1}{3}} \left( \frac{\alpha}{3} \right)^{\frac{1}{4}} \left( \frac{\epsilon}{2} \right)^{\frac{1}{6}} \left( \frac{M_P}{M_{\text{BH}}} \right)^{\frac{5}{6}} T_0 \quad (68)$$

or

$$f_0^{UV} \simeq 4.0 \times 10^6 \left( \frac{1 \text{ g}}{M_{\text{BH}}} \right)^{\frac{5}{6}} \text{ Hz}, \quad (69)$$

which is slightly higher than what we see in Fig. 1. This is due to the non linear cutoff we have used in order to cut the spectra in our numerical analysis to obtain Fig. 1. For the interested reader this issue is discussed in detail in the last part of appendix D. The comparison should be made with the most shaded curve of Fig. 9 which reproduces Fig. 1 with different cutoffs. And this fits well with our analytical result (69). The question on how to estimate the cutoff is still subject to discussions in the literature [78–81]. We have chosen to display the most conservative option in our Fig. 1, but the interested reader can take a look at appendix D and Fig. 9 to appreciate the impact of this choice.

The infrared cutoff of the density fluctuations waves correspond obviously to the (casually connected) size of the horizon at the time of PBH evaporation, or

$$f_{IR} \sim \frac{H(a_{\text{ev}})}{2\pi} = \frac{1}{3\pi} \Gamma_{\text{ev}}, \quad (70)$$

which gives in the semiclassical limit, after redshifting from  $a_{\text{RH}} = a_{\text{ev}}$  to  $a_0$  :

$$f_0^{IR} = \frac{\sqrt{\epsilon}\alpha^{\frac{1}{4}}}{3^{\frac{1}{4}}\sqrt{2\pi}} \left(\frac{M_P}{M_{BH}}\right)^{\frac{3}{2}} \left(\frac{g_0}{g_{RH}}\right)^{\frac{1}{3}} T_0, \quad (71)$$

or

$$f_0^{IR} \simeq 947 \left(\frac{1 \text{ g}}{M_{BH}}\right)^{\frac{3}{2}} \text{ Hz}, \quad (72)$$

which is also what we clearly see in Fig. 1.

The precise shape of the spectrum between  $f_0^{IR}$  and  $f_0^{UV}$  is detailed in appendix D, and necessitates the calculation of complex second order transfer functions from density perturbations to scalar (potential) perturbations and finally tensor (metric) perturbations. For a complete analysis, we refer the reader to the works of [76], [81–83] and [84, 85]. We obtained

$$\Omega_{GW}^{B_1} h^2 \propto \left(\frac{f}{f_{UV}}\right)^{\frac{11}{3}}, \quad (73)$$

for  $f \lesssim f_{UV}$ , and

$$\Omega_{GW}^{B_1} h^2 \sim \left(\frac{f}{f_{UV}}\right), \quad (74)$$

for  $f \gtrsim f_{IR}$ , which is also what we observe in Fig. 1, the change of slope corresponding to the passage from inflaton domination to PBH domination. The break in the spectrum is more visible in Fig. 9.

### C. Burdening the spectrum

The consequence of a memory burden effect on the GW generated by density fluctuations are clearly visible in Fig. 1. As it was the case for the PGW, the UV cutoff part of the spectrum is not *directly* affected by the burdening, because this corresponds roughly to the distance between two PBHs, which is determined at formation time. However, it is the *redshift* of this distance which is affected between  $a_{BH}$  and  $a_{RH}$ , because the PBH domination lasts longer. Using Eq. (66), but with the burdened width  $\Gamma_{BH}$  given in Eq. (15), we obtain

$$\begin{aligned} f_{UV}|_n^q &= \frac{2^{\frac{1}{3}}}{(3\pi)^{\frac{2}{3}}} \left(\frac{M_P^2 \Gamma_{BH}^2}{M_{BH}}\right)^{\frac{1}{3}} \\ &= M_P \left(\frac{2^{n+\frac{1}{2}}(3+2n)\epsilon}{3\pi q^{3+2n}}\right)^{\frac{2}{3}} \left(\frac{M_P}{M_{BH}}\right)^{\frac{7+4n}{3}}, \end{aligned} \quad (75)$$

which gives after redshifting from  $a_{ev}$  to  $a_0$

$$f_0^{UV} = f_{UV} \left(\frac{g_0}{g_{RH}}\right)^{\frac{1}{3}} \frac{T_0}{T_{RH}} = \frac{\alpha^{\frac{1}{4}}}{3^{\frac{5}{12}}} \left(\frac{g_0 \sqrt{M_P \Gamma_{BH}}}{\sqrt{2} g_{RH} \pi^2 M_{BH}}\right)^{\frac{1}{3}} T_0,$$

or

$$f_0^{UV}|_n^q = \frac{\alpha^{\frac{1}{4}} \epsilon^{\frac{1}{6}}}{3^{\frac{5}{12}}} \frac{2^{\frac{n-1}{6}} (3+2n)^{\frac{1}{6}}}{\pi^{\frac{2}{3}} q^{\frac{1}{2}+\frac{n}{3}}} \left(\frac{M_P}{M_{BH}}\right)^{\frac{5}{6}+\frac{n}{3}} \frac{g_0^{\frac{1}{3}}}{g_{RH}^{\frac{1}{3}}} T_0. \quad (76)$$

Note that we recover the expression (68) if one takes  $n=0, q=1$  in Eq. (76). For our benchmark point  $n=1, q=\frac{1}{2}$ , we obtain

$$f_0^{UV}|_{n=1}^{q=\frac{1}{2}} \simeq 1.4 \times 10^5 \left(\frac{1 \text{ g}}{M_{BH}}\right)^{\frac{7}{6}} \text{ Hz}, \quad (77)$$

which is again slightly higher than what we can see in Fig. 1 due to the cutoff issue already discussed in the unburdened case. Nevertheless, this value matches very well with Fig. 9, where the most shaded line released the cutoff constraint.

Concerning the IR cutoff,  $f_0^{IR}$ , it corresponds to the size of the Universe at the time of PBH decay, which is the causally connected region. As in the non-burdened case, this corresponds to  $f_0^{RH}$ , or

$$f_0^{IR}|_n^q = f_0^{RH}|_n^q, \quad (78)$$

where  $f_0^{RH}|_n^q$  is given by Eq. (46). This is indeed what we observe in the region  $B_2$  of Fig. 1. In conclusion, the memory burden effect on the GW generated by the density fluctuations of PBHs is also to enlarge the spectrum toward lower frequencies  $f_0$ . The relation between  $f_0^{IR}$  and  $f_0^{UV}$

$$\frac{f_0^{UV}}{f_0^{IR}}|_n^q \sim \left(\frac{M_{BH}}{M_P}\right)^{\frac{2}{3}(1+n)} q^{1+\frac{2n}{3}}, \quad (79)$$

gives a direct access to the memory burden parameters, allowing to signal the presence of such effects on PBHs from the measurement of the corresponding frequencies. For instance, the ratio  $f_0^{UV}/f_0^{IR} \simeq 4200$  in the semiclassical approach, whereas it is  $\simeq 3.3 \times 10^6$  for our benchmark point  $n=1, q=0.5$ , illustrating the larger

## VI. PRIMORDIAL BLACK HOLES EVAPORATION

### A. The spectrum ( $D_1$ )

Another source of gravitational waves is of course the gravitons directly produced by the evaporation of the

PBHs. If we suppose that the vast majority of them are emitted at the evaporation time  $\Gamma_{\text{BH}}^{-1}$ , we expect a peak at the present epoch for a frequency  $f_0^{\text{ev}}$  corresponding to  $\sim T_{\text{BH}}$  redshifted from  $a_{\text{ev}} = a_{\text{RH}}$  till  $a_0$ . The GW energy density spectrum generated by PBHs decay reaches its maximum for the maximum of the distribution function  $g(X) = \frac{X^3}{e^X - 1}$ , which is obtained for  $X^{\text{peak}} \simeq 2.8$  [30]. Applied to a thermal distribution of gravitons around the PBH,  $d\rho_h \sim \frac{k}{2\pi^2} \times \frac{k^2 dk}{e^{\frac{k}{T_{\text{BH}}}} - 1}$ , this gives

$$\begin{aligned} f_{\text{ev}} \simeq \frac{2.8}{2\pi} T_{\text{BH}} &= \frac{2.8 M_P^2}{2\pi M_{\text{BH}}} \simeq 4.5 \times 10^{12} \left( \frac{1\text{g}}{M_{\text{BH}}} \right) \text{ GeV} \\ &= 6.9 \times 10^{36} \left( \frac{1\text{g}}{M_{\text{BH}}} \right) \text{ Hz}, \end{aligned} \quad (80)$$

which implies

$$f_0^{\text{ev}} = f_{\text{ev}} \frac{g_0^{\frac{1}{3}}}{g_{\text{RH}}^{\frac{1}{3}}} \frac{T_0}{T_{\text{RH}}} = \frac{(3\alpha)^{\frac{1}{4}}}{2^{\frac{3}{2}}\pi} \frac{M_P^{\frac{3}{2}}}{M_{\text{BH}}\sqrt{\Gamma_{\text{BH}}}} \frac{g_0^{\frac{1}{3}}}{g_{\text{RH}}^{\frac{1}{3}}} T_0, \quad (81)$$

where we used Eq. (10). In the semiclassical limit, where  $\Gamma_{\text{BH}}$  is given by Eq. (4), we obtain

$$\begin{aligned} f_0^{\text{ev}} &= \left( \frac{\alpha}{3} \right)^{\frac{1}{4}} \frac{2.8}{2\sqrt{2}\epsilon\pi} \sqrt{\frac{M_{\text{BH}}}{M_P}} \frac{g_0^{\frac{1}{3}}}{g_{\text{RH}}^{\frac{1}{3}}} T_0 \\ &\simeq 1.5 \times 10^{13} \sqrt{\frac{M_{\text{BH}}}{1\text{g}}} \text{ Hz}, \end{aligned} \quad (82)$$

which is effectively what we observe in the region  $D_1$  of Fig. 1.

Note that the evaporation of a black hole does-not produce an exact black body spectrum with a fix temperature  $T_{\text{BH}}$ . Other factors (called "grey-body" factors) need to be taken into account, notably for the possibility of particles reabsorption [45]<sup>6</sup>. The temperature  $T_{\text{BH}}$  itself is not a fixed quantity, but depends on the proper evolution of  $M_{\text{BH}}$  and the redshift (and thus on the main component of the Universe). All these effects have of course been taken into account to produce Fig. 1, and are detailed in the appendix B. That explains the kind of "misshapen" spectrum  $D_1$ , and not a black-body spectrum, we should observe today.

Note also that the gravitational wave amplitude  $\rho_{\text{GW}}$  at the peak of the spectrum  $D_1$ , has a remarkable property: it *does not depend* on the mass of the PBH. We

explain this peculiarity of the spectrum in appendix B 4, but also in Fig. 3, where we considered a set of different values for  $M_{\text{BH}}$ . Without going into the detail of the spectrum of the products from PBH evaporation, we can estimate this peak value,  $\Omega_{\text{GW}}^{D_1}$ , by simple considerations. Indeed, the total number of particles  $N$  produced at  $a_{\text{RH}}$ , should be

$$N \sim \frac{M_{\text{BH}}}{T_{\text{BH}}} = \frac{M_{\text{BH}}^2}{M_P^2} \simeq 5.5 \times 10^{10} \left( \frac{M_{\text{BH}}}{1\text{g}} \right)^2. \quad (83)$$

From these particles, only  $\frac{2}{2+g_{\text{RH}}} \times N$  are gravitons, the rest populate the thermal bath. To estimate the value of  $\frac{d\rho_{\text{GW}}(f)}{df}$  at  $f = f_{\text{ev}} \simeq \frac{2.8}{2\pi} T_{\text{BH}}$ , one can then naively expect, for a PBH reheating, using Eq. (25) with  $\frac{\rho_{\text{GW}}}{\rho_R} = \frac{2}{2+g_{\text{RH}}}$

$$\boxed{\Omega_{\text{GW}}^{D_1} h^2 \simeq 7.5 \times 10^{-7}}, \quad (84)$$

with  $g_{\text{RH}} = 106.75$ .  $\Omega_{\text{GW}}^{D_1}$  is of course independent on  $M_{\text{BH}}$  or  $\beta$ , because the PBH decay does not distinguish gravitons from radiation, up to the number of degrees of freedom. The precise calculation and the corresponding peak values are given in appendix B. This value at the peak, as well as the PGW from inflation Eq. (26), is a clear, model independent signature of a PBH reheating phase. The value corresponds roughly to the one we see in Fig. 1, with some corrections or order unity developed in the appendix B 4. The main difference comes from the fact that the evaporation is not instantaneous, and  $T_{\text{BH}}$  increases when approaching  $a_{\text{ev}}$ , diluting the peak value within a range of higher frequencies, as we can see on the left part of point  $D_1$  in Fig. 1.

The limit of this argument comes from the validity of considering  $M_{\text{BH}}$  as constant. While this approximation stays valid during most of the PBH evaporation, this is not the case that close to evaporation. All the spectra on the right side of the evaporation peak is generated on a timescale much shorter than the Hubble rate. During this period the rapid increase of the PBH temperature distributes the particles over a much larger range of energies, which results in a lower abundance. However since the peak is near the point where  $\Gamma_{\text{BH}}^{(n)} \sim H$  we can still get a fair estimation of the behavior at the peak, Eq. (84), with such a simple argument.

## B. Burdening the spectrum ( $D'_1$ and $D'_2$ )

The memory burden effect should of course also affect the GW spectrum from the PBH decay. As we discussed in section II C, the memory burden acts as if the evaporation happens in two stages, with a transition when  $M_{\text{BH}} = qM_{\text{in}}$ . As a consequence, we expect a spectrum

<sup>6</sup>Note that accounting for general relativistic corrections to the accretion of relativistic matter onto PBHs can enhance their mass growth by an order of magnitude [45, 46, 86, 87] shortly after formation, leading to important phenomenological implications; throughout this analysis, we ignore such effects.

which is a combination of two thermal baths. The first phase corresponds to a PBH decaying with a temperature  $T_{\text{BH}} = \frac{M_P^2}{M_{\text{BH}}}$  at a time  $\Gamma_{\text{BH}}^{-1} \sim \frac{M_{\text{in}}^3}{3\epsilon M_P^4}$ , Eq. (4). This frequency peaks at  $f_{\text{ev}1} \simeq \frac{2.8}{2\pi} T_{\text{BH}}$ , with  $T_{\text{BH}} = \frac{M_P^2}{M_{\text{in}}}$ , see Eq. (80). However, even if this frequency does not feel directly the memory burden effect, the redshift following the first phase does. In other words,

$$f_0^{\text{ev}1}|_n^q = \frac{2.8}{2\pi} \frac{M_P^2}{M_{\text{in}}} \left( \frac{a_{\text{ev}1}}{a_{\text{RH}}} \right) \left( \frac{a_{\text{RH}}}{a_0} \right)$$

or

$$f_0^{\text{ev}1}|_n^q = \frac{2.8}{2\pi} \frac{\alpha^{\frac{1}{4}}}{\sqrt{2\epsilon}} \frac{2^{\frac{n}{6}} (3+2n)^{\frac{1}{6}}}{3^{\frac{5}{12}} q^{\frac{1}{2} + \frac{n}{3}}} \left( \frac{M_P}{M_{\text{in}}} \right)^{\frac{n}{3} - \frac{1}{2}} \frac{g_0^{\frac{1}{3}}}{g_{\text{RH}}^{\frac{1}{3}}} T_0, \quad (85)$$

where we used

$$\frac{a_{\text{ev}1}}{a_{\text{RH}}} = \left( \frac{\rho_{\text{RH}}}{\rho(a_{\text{ev}1})} \right)^{\frac{1}{3}} = \left( \frac{\Gamma_{\text{BH}}^n}{\Gamma_{\text{BH}}} \right)^{\frac{2}{3}}, \quad (86)$$

and

$$\frac{a_{\text{RH}}}{a_0} = \frac{g_0^{\frac{1}{3}}}{g_{\text{RH}}^{\frac{1}{3}}} \frac{T_0}{T_{\text{RH}}} = \frac{g_0^{\frac{1}{3}}}{g_{\text{RH}}^{\frac{1}{3}}} \frac{(3\alpha)^{\frac{1}{4}}}{\sqrt{2}} \frac{T_0}{\sqrt{M_P \Gamma_{\text{BH}}^n}}, \quad (87)$$

$\Gamma_{\text{BH}}^n$  being given by Eq. (15) and  $\Gamma_{\text{BH}}$  by Eq. (4). Of course, we recover Eq. (82) for  $n = 0$ ,  $q = 1$ , whereas for our benchmark point  $n = 1$ ,  $q = \frac{1}{2}$ , we obtain

$$f_0^{\text{ev}1}|_{n=1}^{q=\frac{1}{2}} \simeq 5.4 \times 10^{11} \left( \frac{M_{\text{BH}}}{1\text{g}} \right)^{\frac{1}{6}} \text{Hz}, \quad (88)$$

which is effectively the first peak  $D'_1$  we observe in Fig. 1.

The second peak frequency corresponds to the evaporation of a PBH with a mass  $M_{\text{BH}} = qM_{\text{in}}$ , redshifted from  $a_{\text{RH}}$  to  $a_0$ , or

$$f_0^{\text{ev}2} = \frac{2.8}{2\pi} \frac{M_P^2}{qM_{\text{in}}} \frac{a_{\text{RH}}}{a_0} \quad (89)$$

which gives, using (87),

$$f_0^{\text{ev}2}|_n^q = \frac{2.8}{2\pi} \frac{(3\alpha)^{\frac{1}{4}}}{\sqrt{2\epsilon}} \frac{1}{2^{\frac{n}{2}} \sqrt{3+2n}} \left( \frac{M_P}{qM_{\text{in}}} \right)^{-\frac{1}{2}-n} \frac{g_0^{\frac{1}{3}}}{g_{\text{RH}}^{\frac{1}{3}}} T_0, \quad (90)$$

where we recover also Eq. (82) for  $n = 0$ ,  $q = 1$ , whereas for our benchmark point  $n = 1$ ,  $q = \frac{1}{2}$ , we obtain

$$f_0^{\text{ev}2}|_{n=1}^{q=\frac{1}{2}} \simeq 7 \times 10^{17} \left( \frac{M_{\text{BH}}}{1\text{g}} \right)^{\frac{3}{2}} \text{Hz}, \quad (91)$$

which corresponds to the second peak,  $D'_2$  we see in Fig. 1.

Note that increasing  $M_{\text{BH}}$  pushes the frequency of the first and second peaks toward larger values, but with a different dependence on  $M_{\text{BH}}$ . In another words, a measurement of the two peaks is not only a proof of the existence of a memory burden effect, but also can help to determine the parameters  $n$  and  $q$ . Indeed, if a double-peaked signal is observed, the ratio between the two frequencies

$$\frac{f_0^{\text{ev}2}}{f_0^{\text{ev}1}} \simeq \frac{1.2 q^{1+\frac{4}{3}n}}{(2^n(3+2n))^{\frac{2}{3}}} \left( \frac{M_{\text{in}}}{M_P} \right)^{\frac{4}{3}n-1} \sim \left( \frac{M_{\text{in}}}{M_P} \right)^{\frac{4}{3}n-1}, \quad (92)$$

combined with Eq. (90), gives a direct access to  $n$ .

Concerning the amplitude, the second phase gives rise to the reheating process, and then, all the arguments used to compute  $\Omega_{\text{GW}}^{D'_1}$  are also valid here. A more detailed calculation gives a small dependence of the peak value on the burden parameter  $n$ , and is presented in appendix B4. However, the unburdened computation stay a good approximation even in this case, or

$$\Omega_{\text{GW}}^{D'_2} = \Omega_{\text{GW}}^{D'_1} \simeq 7.5 \times 10^{-7}. \quad (93)$$

This is not the case for the lower frequency peak, generated by the first phase of the evaporation, due to the redshift of  $\rho_{\text{GW}}$  in a matter dominated Universe before  $a_{\text{RH}}$ .

## VII. DEPENDANCE ON $M_{\text{BH}}$ AND $w_\phi$

Our study focused on the benchmark point  $M_{\text{BH}} = 1\text{g}$  and  $w_\phi = \frac{1}{2}$ , to help the reader understand the different regions of the PGW spectrum represented in Fig. 1. We want in this section to complete our study to larger masses and different values of  $\beta$ . We show our result for  $M_{\text{BH}} = 100$  and  $10^4\text{g}$  in Fig. 3, (Fig. 4) in the unburden (burden) case, from the black-dashed line to green-dash-dotted line.

As already discussed in the previous section, concerning the PBH evaporation point  $D_1$ , we observe a slight shift toward larger frequencies for larger masses. This comes from the fact that heavier PBH decays later, limiting the redshift of the gravitons produced from  $a_{\text{RH}}$  to  $a_0$ . On the other hand, for the density fluctuation peak (regions  $B_1$  and  $B_2$ ), we see a large shift toward *lower* frequencies for larger  $M_{\text{BH}}$ . This is due to the fact that

the horizon is larger at evaporation time  $a_{\text{RH}}$  for heavier PBHs. The distance between them, as well as the size of the horizon is then larger, pushing  $f_0^{\text{IR}}$  and  $f_0^{\text{UV}}$  towards lower values.

Concerning the primordial gravitational waves, increasing the mass of PBHs extend the inflaton domination region  $A_3$  because heavier PBH are formed later. As a consequence, the frequency where the PBH dominates the energy budget of the Universe,  $f_0^{\text{BH}}$  is shifted naturally toward lower values, as one can see in the left part of Fig. 3 and Eq. (40). The inflaton scattering can only be modified through the overall redshift effect induced by the PBH domination era which then follows the behavior of the PGW dependence.

If one takes into account the memory burden effect, the conclusions are largely the same, as we show in Fig. 4. Whereas the two peaks generated by the PBHs decay are shifted towards larger frequencies for larger mass due to a reduction of the redshift, the density perturbation spectrum is shifted toward even much lower frequencies than in the non-burden case due to an effective enlargement of the PBH lifetime.

The effect of the value of  $\beta$  is much weaker, as we show in Fig. 5. Whereas the PBH decay spectrum is mainly unchanged, due to the universal nature of the decay into gravitons once PBHs dominate the Universe, as we explained above, the density perturbation spectrum is altered. Smaller  $\beta$  means later domination, or a longer  $\phi$  domination time. In Fig. 5, we also show the influence of the EoS  $w_\phi$  on the GW spectrum for a fixed  $M_{\text{BH}} = 1$  g. The slope of the spectrum range from  $\Omega_{\text{GW}}^{A_3} \propto f_0^{-2}$  before the PBH formation for  $w_\phi = 0$ , to  $\Omega_{\text{GW}}^{A_3} \propto f_0$  for  $w_\phi = 1$ , which is in agreement with our result (44),  $\Omega_{\text{GW}}^{A_3} \propto f_0^{\frac{6w_\phi - 2}{3w_\phi + 1}}$ . Taking into account the memory burden effect, we obtained Fig. 6 for different values of  $w_\phi$ . The dependence on  $w_\phi$  is comparable to the non-burden case.

## VIII. CONCLUSION

Our conclusion can be summarized by Fig. 1, where we show all the sources we took into account to obtain a PGW spectrum in presence of the inflaton field and a population of PBH. Indeed, by its proper nature, gravitational waves have many sources, because any object couples in a way or another, with the metric. In our work, we decided to concentrate on two main sources of gravitational waves : the primordial black holes, and the inflaton field. Our choice was dictated by the fact that these two sources can be considered as a minimal as long as one considers the possibility of inflation and the existence of primordial black hole. Any other extension would generate a spectrum *above* the one we presented in Fig. 1. We also extended our analysis, considering

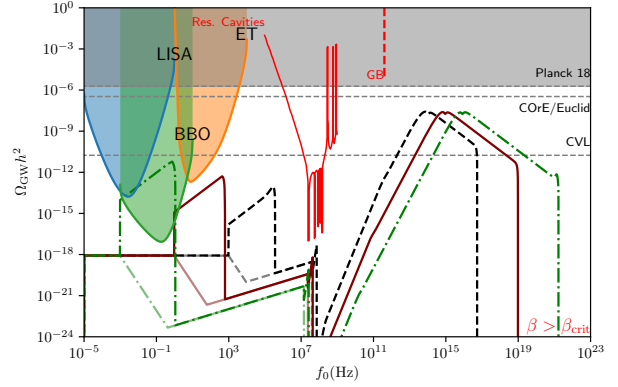


Figure 3. GW spectra in the unburden case with  $w_\phi = 1/2$  for  $M = 1, 10^2$  and  $10^4$  g respectively for black, red and green with  $\beta = 10^{-5}, 10^{-6}$  and  $10^{-7}$

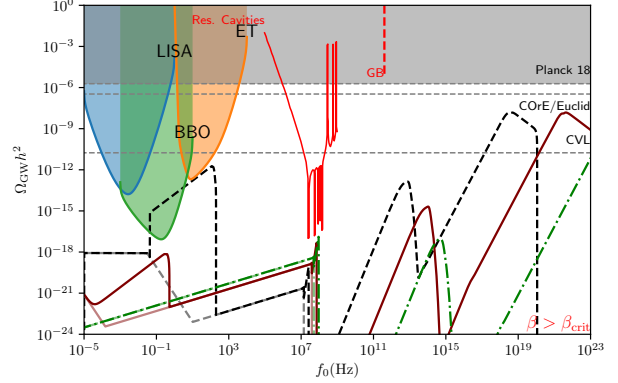


Figure 4. GW spectra in the burden case with  $w_\phi = 1/2$  for  $M = 1, 10^2$  and  $10^4$  g respectively for black, red and green with  $\beta = 10^{-8}, 10^{-13}$  and  $10^{-17}$

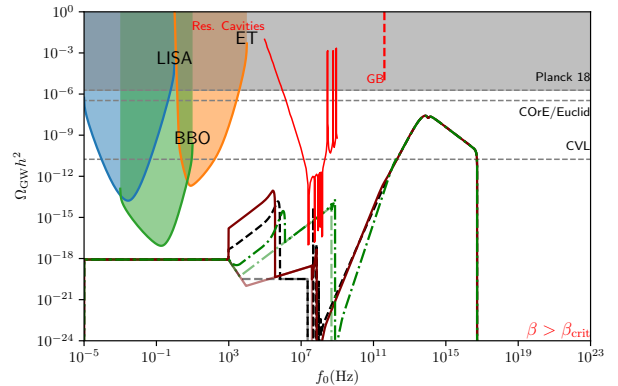


Figure 5. GW spectra in the unburdened case with  $w_\phi = 1/3, 1/2$  and  $1$  respectively for black, red and green with  $\beta = 10^{-4}, 10^{-5}$  and  $10^{-9}$ . The PBH mass is fixed to  $M = 1$  g



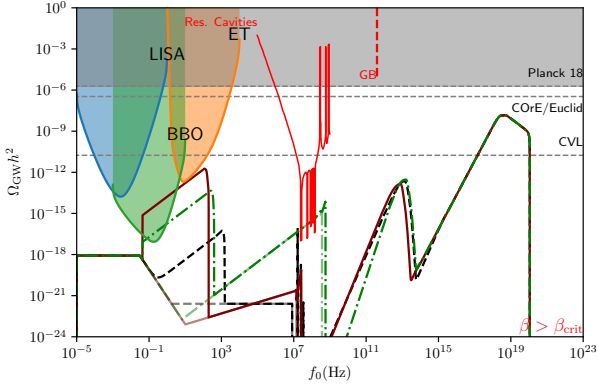


Figure 6. GW spectra in the burden case with  $w_\phi = 1/3, 1/2$  and  $1$  respectively for black, red and green with  $\beta = 10^{-7}, 10^{-8}$  and  $10^{-13}$ . The PBH mass is fixed to  $M = 1g$

the possibility of memory burden effects in the process of PBH evaporation.

We then distinguished typical signatures in the spectrum, characteristic of the different gravitational wave sources. Having access to the spectrum of primordial gravitational waves is like reading the history of the Universe from inflation to the CMB. We can guess the species which dominates the evolution at each stage, recognize the presence of primordial holes, and even measure the reheating temperature. For all these reasons, we consider that the hunt for primordial gravitational waves is one of the major objectives of our discipline for the decades to come.

## ACKNOWLEDGMENTS

The authors want to warmly thank Donald Kpataha, Simon Clery, Vincent Vennin and Lucien Heurtier for extremely useful discussions, especially during the Astro@Paris-Saclay symposium 2024 and the "Gravitational Probes of the Early Universe" workshop at King's College, London in 2025. This project has received funding from the European Union's Horizon Europe research and innovation programme under the Marie Skłodowska-Curie Staff Exchange grant agreement No 101086085 – ASYMMETRY and the CNRS-IRP project UCMN. MRH thanks ISI, Kolkata, for financial support through Research Associateship.

## APPENDIX

### Appendix A: Primordial gravitational wave spectrum: a primer

#### 1. The spectrum

For the reader interested by a detailed analysis of the PGW spectrum, we refer to [61, 88–94]. The aim of this appendix is to give to the reader the necessary tools to understand section III. Here, primordial gravitational waves refer to those generated as tensor perturbations due to vacuum fluctuations during inflation, in the absence of any source terms. These fluctuations are described by the perturbed FLRW metric

$$ds^2 = a^2(\eta) [d\eta^2 - (\delta_{ij} + h_{ij}) dx^i dx^j], \quad (\text{A1})$$

where  $h_{ij}$  is transverse and traceless. In Fourier space, the mode equation for  $h_k$  reads

$$h_k'' + 2\frac{a'}{a}h_k' + k^2 h_k = 0. \quad (\text{A2})$$

Defining the Mukhanov-Sasaki variable  $u_k = ah_k$ , the evolution becomes

$$u_k'' + \left(k^2 - \frac{a''}{a}\right) u_k = 0. \quad (\text{A3})$$

Assuming de Sitter inflation, the scale factor is  $a_I(\eta) = -1/(H_I\eta)$ <sup>7</sup>, yielding a nearly scale-invariant power spectrum

$$\mathcal{P}_T(k) = \frac{4k^3}{2\pi^2} |h_k|^2 \simeq \frac{H_I^2}{2\pi^2 M_P^2} \left(1 + \frac{k^2}{k_{\text{end}}^2}\right), \quad (\text{A4})$$

where  $k_{\text{end}}$  is the comoving scale crossing the horizon at the end of inflation. We focus on the leading term  $k \ll k_{\text{end}}$ , where the spectrum is nearly flat. To track GW evolution post-inflation, we factor out the inflationary mode amplitude:  $h_k(\eta) = h_k(\eta_{\text{end}}) \chi_k(\eta)$ , where  $\chi_k$  evolves through reheating and radiation eras. The transfer function satisfies:

$$\chi_k'' + 2\frac{a'}{a}\chi_k' + k^2 \chi_k = 0. \quad (\text{A5})$$

During reheating, dominated by an equation of state  $w_\phi$ , the Hubble parameter evolves as  $H = H_{\text{end}}(a/a_{\text{end}})^{-\frac{3(1+w_\phi)}{2}}$ . The Eq. (A5) then becomes

<sup>7</sup>Note that we assume the Hubble parameter remains approximately constant during inflation. For slow-roll inflationary models, its variation is negligible, so we set its value at the end of inflation, denoted as  $H_I \simeq H_{\text{end}}$ .

$$\chi_k'' + \frac{5-3w_\phi}{2(a/a_{\text{end}})}\chi_k' + \frac{(k/k_{\text{end}})^2}{(a/a_{\text{end}})^{1-3w_\phi}}\chi_k = 0, \quad (\text{A6})$$

whose solution is the Bessel-function

$$\chi_k^{\text{RH}}(a) = (a/a_{\text{end}})^{-\nu} [C_{1k}J_{-\nu/\gamma}(x) + C_{2k}J_{\nu/\gamma}(x)],$$

where  $\nu = \frac{3}{4}(1-w_\phi)$ ,  $\gamma = \frac{1}{2}(1+3w_\phi)$ , and  $x = k(a/a_{\text{end}})^\gamma/(\gamma k_{\text{end}})$ . Matching conditions at the end of inflation determine  $C_{1k}$  and  $C_{2k}$ ,

$$C_{1k} = \frac{\pi^2}{2\gamma k_{\text{end}}} \left[ \frac{k}{ik - k_{\text{end}}} J_{\frac{\nu}{\gamma}} \left( \frac{k}{\gamma k_{\text{end}}} \right) - J_{\frac{\gamma+\nu}{\gamma}} \left( \frac{k}{\gamma k_{\text{end}}} \right) \right] \quad (\text{A7})$$

$$C_{2k} = \frac{\pi^2}{2\gamma k_{\text{end}}} \left[ \frac{k}{ik - k_{\text{end}}} J_{-\frac{\nu}{\gamma}} \left( \frac{k}{\gamma k_{\text{end}}} \right) - J_{-\frac{\gamma+\nu}{\gamma}} \left( \frac{k}{\gamma k_{\text{end}}} \right) \right] \quad (\text{A8})$$

$$\text{csc} \left( \frac{\pi\nu}{\gamma} \right).$$

where  $\text{csc}$  stands for the cosecant of the product  $\pi\nu/\gamma$ ,  $\text{csc}(\pi\nu/\gamma) = \frac{1}{\sin(\pi\nu/\gamma)}$ . During radiation domination,  $H \propto a^{-2}$ , and the solution becomes

$$\chi_k^{\text{RD}}(a) = \frac{1}{a_{\text{end}}} \left[ D_{1k} e^{\frac{-ik - \frac{a}{a_{\text{end}}}}{k_{\text{RH}} \frac{a_{\text{RH}}}{a_{\text{end}}}}} + D_{2k} e^{\frac{ik - \frac{a}{a_{\text{end}}}}{k_{\text{RH}} \frac{a_{\text{RH}}}{a_{\text{end}}}}} \right]. \quad (\text{A9})$$

As usual, the coefficients  $D_{1k}$  and  $D_{2k}$  are determined by matching the mode solutions and their derivatives at reheating, and are given by

$$D_{1k} = \frac{a_{\text{RH}}/a_{\text{end}}}{2} e^{ik/k_{\text{RH}}} \left[ \left( 1 + \frac{ik_{\text{RH}}}{k} \right) \chi_k^{\text{RH}}(a_{\text{RH}}) + i \frac{k_{\text{RH}}}{k} \frac{a_{\text{RH}}}{a_{\text{end}}} \frac{\partial \chi_k^{\text{RH}}(a_{\text{RH}})}{\partial (a/a_{\text{end}})} \right] = i \frac{(a_{\text{RH}}/a_{\text{end}})k_{\text{RH}}}{2k} \mathcal{E}_{1k}. \quad (\text{A10})$$

$$D_{2k} = \frac{a_{\text{RH}}/a_{\text{end}}}{2} e^{-ik/k_{\text{RH}}} \left[ \left( 1 - \frac{ik_{\text{RH}}}{k} \right) \chi_k^{\text{RH}}(a_{\text{RH}}) - i \frac{k_{\text{RH}}}{k} \frac{a_{\text{RH}}}{a_{\text{end}}} \frac{\partial \chi_k^{\text{RH}}(a_{\text{RH}})}{\partial (a/a_{\text{end}})} \right] = -i \frac{(a_{\text{RH}}/a_{\text{end}})k_{\text{RH}}}{2k} \mathcal{E}_{2k}. \quad (\text{A11})$$

Deep inside the radiation-dominated era, the gravitational wave energy density per logarithmic interval is given by:

$$\rho_{\text{GW}}(k, \eta) = \frac{M_{\text{p}}^2 k^2 a_{\text{end}}^2}{4a^4} \mathcal{P}_T(k) (|D_{1k}|^2 + |D_{2k}|^2). \quad (\text{A12})$$

Normalizing to the critical density  $\rho_c = 3M_{\text{p}}^2 H^2$ , the dimensionless density parameter is:

$$\Omega_{\text{GW}}(k, \eta) = \frac{\mathcal{P}_T(k)}{48} (|\mathcal{E}_{1k}|^2 + |\mathcal{E}_{2k}|^2). \quad (\text{A13})$$

At late times, the redshifting leads to

$$\Omega_{\text{GW}}(k) h^2 = c_g \Omega_{\text{rad},0} h^2 \Omega_{\text{GW}}(k, \eta), \quad (\text{A14})$$

where  $c_g \sim 0.4$  accounts for changes in relativistic degrees of freedom. The current radiation energy density, including photons and three neutrino species, is given by  $\Omega_{\text{rad},0} h^2 = 4.16 \times 10^{-5}$ . In the long-wavelength limit  $k \ll k_{\text{RH}}$ , the mode functions satisfy  $|\mathcal{E}_{1k}|^2 = |\mathcal{E}_{2k}|^2 \simeq 1$ , indicating no spectral distortion. However, in the short-wavelength limit  $k \gg k_{\text{RH}}$ , the amplitude exhibits scale-dependent enhancement,

$$|\mathcal{E}_{1k}|^2 = |\mathcal{E}_{2k}|^2 = \frac{4\gamma^2}{\pi} \Gamma^2 \left( 1 + \frac{\nu}{\gamma} \right) \left( \frac{k}{2\gamma k_{\text{RH}}} \right)^{n_{\text{GW}}} \quad (\text{A15})$$

where the spectral index is

$$n_{\text{GW}} = 1 - \frac{2\nu}{\gamma} = -\frac{2(1-3w_\phi)}{1+3w_\phi}. \quad (\text{A16})$$

This spectral tilt arises from the redshifting of modes relative to the background during reheating and is determined by the effective equation of state  $w_\phi$ . The present-day GW energy density spectrum is then given by

$$\Omega_{\text{GW}}^{\text{rad}}(k) h^2 = \frac{\Omega_{\text{rad},0} h^2}{12\pi^2} \frac{H_{\text{end}}^2}{M_{\text{p}}^2}, \quad \text{for } k \ll k_{\text{RH}}, \quad (\text{A17})$$

and in the high-frequency regime  $k \gg k_{\text{RH}}$ , it becomes

$$\Omega_{\text{GW}}(k) h^2 = \Omega_{\text{GW}}^{\text{rad}}(k) h^2 \cdot \frac{4\gamma^2}{\pi} \Gamma^2 \left( 1 + \frac{\nu}{\gamma} \right) \left( \frac{k}{2\gamma k_{\text{RH}}} \right)^{n_{\text{GW}}}. \quad (\text{A18})$$

This expression encapsulates the effect of reheating dynamics on the high-frequency tail of the GW spectrum, which varies with the background equation of state: it is red-tilted ( $n_{\text{GW}} < 0$ ) for  $w_\phi < 1/3$ , scale-invariant ( $n_{\text{GW}} = 0$ ) for  $w_\phi = 1/3$ , and blue-tilted ( $n_{\text{GW}} > 0$ ) for  $w_\phi > 1/3$ . For example, matter-like reheating with  $w_\phi = 0$  leads to  $n_{\text{GW}} = -2$ , while a kination-dominated phase with  $w_\phi = 1$  yields  $n_{\text{GW}} = 1$ .

## 2. Constraints on reheating

For a stiff post-inflationary equation of state, the reheating temperature  $T_{\text{RH}}$  can be constrained by the additional relativistic degrees of freedom sourced by gravitational waves. We now analyze how small  $T_{\text{RH}}$  can be while remaining consistent with bounds on  $\Delta N_{\text{eff}}$ , assuming fixed values of the equation of state  $w_\phi$  and the

inflationary energy scale. Here,  $\Delta N_{\text{eff}}$  quantifies the excess relativistic degrees of freedom at the epochs of Big Bang Nucleosynthesis (BBN) or CMB decoupling. For a stochastic GW background, the contribution to  $\Delta N_{\text{eff}}$  is given by [95]

$$\Delta N_{\text{eff}} = \frac{\rho_{GW}}{\rho_\nu} = \frac{8}{7} \left( \frac{11}{4} \right)^{4/3} \frac{\rho_{GW}}{\rho_\gamma}, \quad (\text{A19})$$

where  $\rho_\nu$  and  $\rho_\gamma$  denote the energy densities of a single neutrino species and photons, respectively. This expression uses the standard relation  $T_\nu = (4/11)^{1/3} T_\gamma$ . Equation (A19) imposes an upper limit on the total GW energy density today

$$\int_{k_{\text{RH}}}^{k_{\text{end}}} \frac{dk}{k} \Omega_{GW}(k) h^2 \leq \frac{7}{8} \left( \frac{4}{11} \right)^{4/3} \Omega_\gamma h^2 \Delta N_{\text{eff}}, \quad (\text{A20})$$

where the present-day photon energy density is  $\Omega_\gamma h^2 \simeq 2.47 \times 10^{-5}$ . For blue-tilted spectra ( $w_\phi > 1/3$ ), the GW energy is dominated by modes near  $k_{\text{end}}$ , which exited the Hubble horizon at the end of inflation and reentered shortly after. In this regime, substituting the GW spectrum from Eq. (A18) into Eq. (A20) and integrating yields

$$\int_{k_{\text{RH}}}^{k_{\text{end}}} \frac{dk}{k} \Omega_{GW}(k) h^2 \simeq \Omega_{GW}^{\text{rad}} h^2 \zeta(w_\phi) \left( \frac{k_{\text{end}}}{k_{\text{RH}}} \right)^{\frac{6w_\phi - 2}{1+3w_\phi}}, \quad (\text{A21})$$

where

$$\zeta(w_\phi) = (1 + 3w_\phi)^{\frac{4}{1+3w_\phi}} \Gamma^2 \left( \frac{5 + 3w_\phi}{2 + 6w_\phi} \right) \frac{1 + 3w_\phi}{2\pi(3w_\phi - 1)}. \quad (\text{A22})$$

The ratio between the comoving scales  $k_{\text{end}}$  and  $k_{\text{RH}}$  is determined by reheating dynamics:

$$\frac{k_{\text{end}}}{k_{\text{RH}}} = \left( \frac{30 \rho_{\text{end}}}{\pi^2 g_{RH}} \right)^{\frac{1+3w_\phi}{6(1+w_\phi)}} T_{\text{RH}}^{-\frac{2}{3} \frac{1+3w_\phi}{1+w_\phi}}, \quad (\text{A23})$$

where  $\rho_{\text{end}} = 3M_{\text{p}}^2 H_{\text{end}}^2$  is the energy density at the end of inflation. Combining Eqs. (A20), (A21), and (A23), we obtain a lower bound on the reheating temperature:

$$T_{\text{RH}} \geq \left( \frac{\Omega_{GW}^{\text{rad}} h^2 \zeta(w_\phi)}{5.61 \times 10^{-6} \Delta N_{\text{eff}}} \right)^{\frac{3(1+w_\phi)}{4(3w_\phi - 1)}} \left( \frac{30 \rho_{\text{end}}}{\pi^2 g_{RH}} \right)^{1/4}. \quad (\text{A24})$$

Here, we assume that the degrees of freedom associated with the thermal bath and entropy are the same at the end of reheating, denoted by  $g_{RH}$ .

### 3. PBH domination

Up to this point, we have considered a scenario where PBHs do not dominate the energy density before evaporating. However, if the initial PBH fraction  $\beta$  exceeds

a critical threshold  $\beta_c$ , the constraint on the reheating temperature  $T_{\text{RH}}$  given in Eq. (A24) can be relaxed. This is because in a PBH-dominated phase, typically a matter-dominated era sandwiched between a radiation-dominated (RD) phase and a  $w_\phi$  dominated phase, the spectral behavior of the gravitational wave relic changes, with  $\Omega_{GW} h^2 \sim k^{-2}$ . As a result, the stringent constraints from  $\Delta N_{\text{eff}}$ , can be avoided if the PBH domination lasts sufficiently long. A rough consistency check with the  $\Delta N_{\text{eff}}$  bound can be performed by evaluating the gravitational wave relic abundance at the high-frequency end of the spectrum,  $k_{\text{end}}$ . The requirement is that it satisfies the inequality:

$$\Omega_{GW}(k_{\text{end}}) h^2 \leq \frac{7}{8} \left( \frac{4}{11} \right)^{4/3} \Omega_\gamma h^2 \Delta N_{\text{eff}} \sim 9.5 \times 10^{-7}, \quad (\text{A25})$$

where we have used the latest bound on  $\Delta N_{\text{eff}}$  from the P-ACT-LB dataset, which imposes the constraint  $\Delta N_{\text{eff}} < 0.17$  at 95% confidence level [96, 97]. In the presence of PBH domination, the spectral behavior of gravitational waves during the  $w_\phi$ -dominated era is

$$\Omega_{GW}(k) h^2 \sim \Omega_{GW}^{\text{rad}} h^2 \cdot \frac{\Gamma(\frac{5}{2})^2}{\pi} \left( \frac{k_{\text{BH}}}{k_{\text{RH}}} \right)^{-2} \left( \frac{k}{k_{\text{BH}}} \right)^{n_{\text{GW}}}. \quad (\text{A26})$$

Therefore, to estimate the gravitational wave relic abundance at  $k_{\text{end}}$ , one simply substitutes  $k = k_{\text{end}}$  in the above expression. The relevant wavenumber ratios in this context take the following form:

$$\frac{k_{\text{BH}}}{k_{\text{RH}}} = \sqrt{2} \beta^{\frac{1+w_\phi}{6w_\phi}} \cdot \left( \frac{2\pi \gamma M_{\text{in}}^2}{\epsilon M_{\text{P}}^2} \right)^{1/3}, \quad (\text{A27})$$

$$\frac{k_{\text{end}}}{k_{\text{BH}}} = \left( \frac{a_{\text{BH}}}{a_{\text{end}}} \right)^{\frac{1+3w_\phi}{2}}, \quad (\text{A28})$$

where,  $\left( \frac{a_{\text{BH}}}{a_{\text{end}}} \right) = \left( \frac{M_{\text{in}} \sqrt{\rho_{\text{end}}}}{4\pi \gamma \sqrt{3} M_{\text{P}}^3} \right)^{\frac{2}{3(1+w_\phi)}} \beta^{-\frac{1}{3w_\phi}}$ . Upon substituting the wave number ratios into the gravitational wave spectrum expression, Eq.(A26), one obtains

$$\begin{aligned} \Omega_{GW}(k_{\text{end}}) h^2 &\simeq \Omega_{GW}^{\text{rad}} h^2 \cdot \frac{3^{\frac{7+3w_\phi}{3(1+w_\phi)}}}{2^{\frac{13+29w_\phi}{3(1+w_\phi)}}} \left( \frac{M_{\text{P}}}{M_{\text{in}}} \right)^{\frac{2(3-w_\phi)}{3(1+w_\phi)}} \\ &\times \frac{\epsilon^{2/3}}{(\pi \gamma)^{\frac{8w_\phi}{3(1+w_\phi)}}} \left( \frac{\rho_{\text{end}}}{M_{\text{P}}^4} \right)^{\frac{3w_\phi - 1}{3(1+w_\phi)}} \beta^{-\frac{4}{3}}. \end{aligned} \quad (\text{A29})$$

The above relic abundance must remain below the upper limit set by the bound on  $\Delta N_{\text{eff}}$ , which is approximately  $10^{-6}$ , corresponding to  $\Delta N_{\text{eff}} = 0.17$ . This constraint on the gravitational wave relic abundance can be translated into an upper bound on the reheating temperature. Utilizing Eq. (10), one finds

$$\frac{T_{\text{RH}}}{M_P} \leq \frac{2^{\frac{5(9+17w_\phi)}{4(3-w_\phi)}}}{3^{\frac{9+5w_\phi}{2(3-w_\phi)}}} \left( \frac{10^{-6}}{\Omega_{\text{GW}}^{\text{rad}} h^2} \right)^{\frac{9(1+w_\phi)}{4(3-w_\phi)}} \left( \frac{\rho_{\text{end}}}{M_P^4} \right)^{\frac{3(1-3w_\phi)}{4(3-w_\phi)}} \quad (\text{A30})$$

$$\times \beta^{\frac{3(1+w_\phi)}{3-w_\phi}} \left( \frac{\pi\gamma}{\epsilon^{1/3}} \right)^{\frac{6w_\phi}{3-w_\phi}} \alpha^{-1/4}.$$

#### 4. Including the memory burden effect

Now, let us modify the scenario by considering a *phase of memory burden* that sets in after the black hole has lost a fraction  $q$  of its initial mass, instead of using the standard semiclassical approximation (i.e., Hawking evaporation). In this framework, the mass dissipation rate is suppressed by the black hole entropy as  $\sim 1/S^n$  (for details, see the next section). Under this assumption, the ratio of the relevant wave numbers is modified and can be expressed as:

$$\frac{k_{\text{BH}}}{k_{\text{RH}}} = \begin{cases} \sqrt{2}\beta^{\frac{1+w_\phi}{6w_\phi}} \left[ \frac{6\pi\gamma}{2^n\epsilon(3+2n)} \left( \frac{qM_{\text{in}}}{M_P} \right)^{2(1+n)} \right]^{\frac{1}{3}}, & \text{for } \beta > \beta_*, \\ \sqrt{2}(q\beta)^{\frac{1+w_\phi}{6w_\phi}} \left[ \frac{6\pi\gamma}{2^n\epsilon(3+2n)} \left( \frac{qM_{\text{in}}}{M_P} \right)^{2(1+n)} \right]^{\frac{1}{3}}, & \text{for } \beta < \beta_*, \end{cases} \quad (\text{A31})$$

and

$$\frac{k_{\text{end}}}{k_{\text{BH}}} = \begin{cases} \frac{\beta^{-\frac{1+3w_\phi}{6w_\phi}}}{(4\pi\sqrt{3}\gamma)^{\frac{1+3w_\phi}{3(1+w_\phi)}}} \left( \frac{M_P}{M_{\text{in}}} \right)^{-\frac{1+3w_\phi}{3(1+w_\phi)}} \left( \frac{\rho_{\text{end}}}{M_P^4} \right)^{\frac{1+3w_\phi}{6(1+w_\phi)}}, \\ \frac{(q\beta)^{-\frac{1+3w_\phi}{6w_\phi}}}{(4\pi\sqrt{3}\gamma)^{\frac{1+3w_\phi}{3(1+w_\phi)}}} \left( \frac{M_P}{M_{\text{in}}} \right)^{-\frac{1+3w_\phi}{3(1+w_\phi)}} \left( \frac{\rho_{\text{end}}}{M_P^4} \right)^{\frac{1+3w_\phi}{6(1+w_\phi)}}, \end{cases} \quad (\text{A32})$$

where the first expression applies for  $\beta > \beta_*$ , and the second for  $\beta < \beta_*$ . Here,  $\beta_*$  is the critical threshold that determines when the memory burden effect sets in. For  $\beta > \beta_*$ , the burden effect occurs during the PBH-dominated phase. Otherwise, it takes place before PBHs come to dominate the energy density of the universe. The value of  $\beta_*$  can be estimated by equating the onset time of the burden effect,  $t_q = \frac{(1-q^3)M_{\text{in}}^3}{3\epsilon M_P^4}$  with the time at which

early matter domination begins,  $t_{\text{BH}} \sim t_{\text{in}} \beta^{-\frac{1+w_\phi}{2w_\phi}}$ . This yields

$$\beta_* = \left[ \frac{\epsilon}{4\pi\gamma(1+w_\phi)(1-q^3)S(M_{\text{in}})} \right]^{\frac{2w_\phi}{1+w_\phi}}. \quad (\text{A33})$$

At this point, we note that throughout the analysis, we assume a scenario in which the memory burden effect begins during the PBH-dominated era. Although in some cases the starting point of burden effect may commence during the inflaton-dominated phase, determined

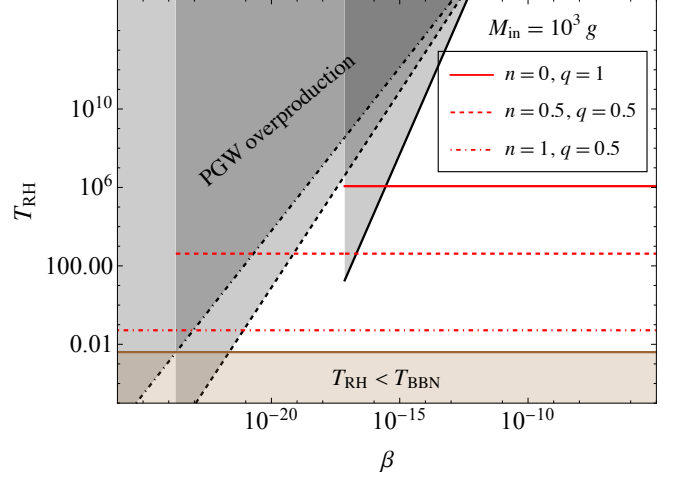


Figure 7. The restriction on the reheating temperature for  $\beta > \beta_c^n$  (i.e., when PBH domination occurs before evaporation) derived from the constraints on  $\Delta N_{\text{eff}}$  via PGWs as a function of  $\beta$  is shown here. The plot includes standard Hawking evaporation ( $n = 0, q = 1$ ) and two combinations of memory burden parameters, namely ( $n = 1/2, q = 1/2$ ) and ( $n = 1, q = 1/2$ ), depicted by the solid, dashed, and dot-dashed black curves, respectively. The black shaded region indicates where PGWs are overproduced, while the red curves denote the corresponding reheating temperatures for the PBH reheating scenario. The brown shaded region indicates reheating temperatures below the BBN energy scale,  $T_{\text{RH}} < T_{\text{BBN}} \sim 4 \text{ MeV}$  [98–100], which are excluded by nucleosynthesis constraints.

by the equation of state  $w_\phi$ , the resulting correction enters through the  $q$ -factor, which affects the spectrum. Since this correction is typically small, we neglect such cases. Finally, the constraint on  $T_{\text{RH}}$  can be obtained by taking into account the overproduction of PGWs followed by the Eq. (A25), leads to the following condition<sup>8</sup>:

$$\frac{T_{\text{RH}}}{M_P} \leq \frac{2^{\frac{5(9+17w_\phi)+6n(5+9w_\phi)}{4(3-w_\phi)+8n(1+w_\phi)}}}{3^{\frac{9+w_\phi+2n(3+w_\phi)}{2(3-w_\phi)+4n(1+w_\phi)}}} \left( \frac{10^{-6}}{\Omega_{\text{GW}}^{\text{rad}} h^2} \right)^{\frac{3(1+w_\phi)(3+2n)}{4(3-w_\phi)+8n(1+w_\phi)}} \quad (\text{A34})$$

$$\left( \frac{\rho_{\text{end}}}{M_P^4} \right)^{\frac{(3+2n)(1-3w_\phi)}{4(3-w_\phi)+8n(1+w_\phi)}} \times \beta^{\frac{(3+2n)(1+w_\phi)}{3-w_\phi+2n(1+w_\phi)}}$$

$$\left( \frac{\pi\gamma}{[\epsilon(3+2n)]^{\frac{1}{3+2n}}} \right)^{\frac{2w_\phi(3+2n)}{3-w_\phi+2n(1+w_\phi)}} q^{\frac{(3+2n)(3w_\phi-1)}{6-2w_\phi+4n(1+w_\phi)}} \alpha^{1/4}.$$

Now let us examine how the constraint behaves in the PBH reheating scenario, where  $\beta > \beta_c^n$  (see, Fig.7),

<sup>8</sup>Note that Eq. (A34) is not exactly accurate for the scenario  $\beta < \beta_*$ , as there will be a correction factor of  $q^{\frac{3(3+2n)(1+w_\phi)}{6-2w_\phi+4n(1+w_\phi)}}$ . However, we ignore this correction since it does not significantly affect the constraint.

which is the focus of this study. We observe that for values of  $\beta$  close to  $\beta_c^n$ , the reheating temperature in PBH reheating scenario can potentially conflict with the  $\Delta N_{\text{eff}}$  bound. However, for larger  $\beta$ , corresponding to a prolonged period of PBH domination, this constraint becomes less stringent. This is because the PBH-dominated era effectively behaves as a matter-dominated phase, during which the gravitational wave background scales as  $\Omega_{\text{GW}} h^2 \propto k^{-2}$ , suppressing the PGW contribution at high frequencies and evading the  $\Delta N_{\text{eff}}$  bound.

## Appendix B: PBH evaporation

### 1. PBH reheating

After inflation ends, the inflaton field typically undergoes coherent oscillations around the minimum of its potential. The effective background equation of state,  $w_\phi$ , depends on the shape of the potential, while the reheating duration is controlled by how rapidly the inflaton decays into Standard Model particles. In the standard picture, the Universe becomes radiation-dominated (RD) once the inflaton decays completely and its energy is transferred to relativistic species [69, 70, 72, 73, 101, 102].

In contrast to the standard reheating scenario, we consider a non-standard post-inflationary history in which primordial black holes (PBHs) form during an inflaton-dominated epoch, and their subsequent evaporation gives rise to a radiation-dominated universe—a scenario referred to as *PBH reheating* [16]. A typical realization of this scenario occurs when the initial PBH abundance parameter  $\beta$  exceeds a critical threshold  $\beta_c$ . In this case, since PBHs behave as non-relativistic matter, they redshift more slowly than the inflaton background with an equation of state  $w_\phi > 0^9$ , allowing PBHs to eventually dominate the energy density before they evaporate, thus initiating the radiation-dominated era [16, 104–107].<sup>10</sup>

Even when PBHs do not dominate the energy density, i.e., for  $\beta < \beta_c$ , reheating can still occur through PBH evaporation. In such cases, unlike scenarios where PBHs dominate prior to evaporation, PBHs form and evaporate during the inflaton-dominated epoch without ever becoming the Universe's main energy component. Reheating via PBH evaporation under these conditions is only possible if the inflaton behaves like a stiff fluid, meaning its equation of state satisfies  $\omega > 1/3$ , and if the inflaton decay or scattering rate remains sufficiently small.

Specifically, the inequality  $\Gamma_\phi \rho_\phi (1 + \omega) < -\frac{\rho_{\text{BH}}}{M_{\text{BH}}} \frac{dM_{\text{BH}}}{dt}$  must be satisfied (see Refs. [16, 28] for details). For the purposes of this study, we exclude this reheating scenario from our analysis.

The PBH evolution is governed by their formation mass  $M_{\text{in}}$  and initial energy fraction  $\beta$ . Assuming ultralight PBHs form in a  $w_\phi$ -dominated background, the evolution equations are:

$$\frac{d\rho_\phi}{da} + 3(1 + w_\phi) \frac{\rho_\phi}{a} = -\frac{\Gamma_\phi \rho_\phi (1 + w_\phi)}{aH}, \quad (\text{B1})$$

$$\frac{d\rho_r}{da} + 4 \frac{\rho_r}{a} \simeq -\frac{\rho_{\text{BH}}}{M_{\text{BH}}} \frac{dM_{\text{BH}}}{da}, \quad (\text{B2})$$

$$\frac{d\rho_{\text{BH}}}{da} + 3 \frac{\rho_{\text{BH}}}{a} = \frac{\rho_{\text{BH}}}{M_{\text{BH}}} \frac{dM_{\text{BH}}}{da}, \quad (\text{B3})$$

$$\frac{dM_{\text{BH}}}{da} = -\epsilon \frac{M_p^4}{M_{\text{BH}}^2} \frac{1}{aH}. \quad (\text{B4})$$

Here,  $\epsilon = \left(\frac{27}{4}\right) \left(\frac{\pi}{480}\right) g_*(T_{\text{BH}})$ , where the factor  $27/4$  originates from the greybody factor. This expression assumes that the greybody factor is evaluated in the geometrical-optics limit, as discussed in Refs. [43, 108, 109]. In our case, we assumed that the radiation primarily comes from PBH evaporation, as inflaton decay is negligible ( $\Gamma_\phi \ll H$ ).

Solving the mass loss equation gives:

$$M_{\text{BH}} = M_{\text{in}} (1 - \Gamma_{\text{BH}}(t - t_{\text{in}}))^{1/3}, \quad \Gamma_{\text{BH}} = \frac{3\epsilon M_p^4}{M_{\text{in}}^3}. \quad (\text{B5})$$

The PBH lifetime is  $t_{\text{ev}} = 1/\Gamma_{\text{BH}}$ , whereas the formation mass is given by

$$M_{\text{in}} = \frac{4\pi\gamma M_p^2}{H_{\text{in}}}, \quad \text{with } \gamma = w_\phi^{3/2}, \quad (\text{B6})$$

following the Carr-Hawking collapse efficiency [110]<sup>11</sup>.

The standard Hawking evaporation neglects backreaction from emitted radiation, but Dvali et al. [47, 50] showed this becomes relevant when the emitted quanta's energy is comparable to the black hole's. This leads to the *memory burden effect* [50], where systems with large information content resist decay until memory is transferred. Once about half the BH mass is lost, stored information slows further evaporation. This modifies PBH mass loss to [17]

<sup>9</sup>Exact matter domination with  $w = 0$  is excluded, as PBH formation in that regime is inefficient due to the long timescales required to form an apparent horizon [103].

<sup>10</sup>Note that,  $w_\phi < 1/3$ , the inflaton is assumed to decay during the PBH-dominated phase, governed by its decay width. For  $w_\phi > 1/3$ , the inflaton must remain stable at least until the onset of PBH domination to ensure consistency with the cosmological framework.

<sup>11</sup>A more accurate determination of the PBH formation mass depends on both the background equation of state  $w_\phi$  and the shape of the primordial perturbations, as shown in Refs. [103, 111–117]. However, a complete analytical treatment of the collapse efficiency parameter  $\gamma$  in the post-inflationary regime is still lacking. Therefore, we adopt the conventional estimate proposed by Carr and Hawking.



$$\frac{dM_{\text{BH}}}{da} = -\frac{\epsilon}{[S(M_{\text{BH}})]^n} \frac{M_P^4}{M_{\text{BH}}^2} \frac{1}{aH}, \quad (\text{B7})$$

with entropy  $S = \frac{1}{2}(M_{\text{BH}}/M_P)^2$  and memory parameter  $n > 0$ . The effect becomes significant when  $M_{\text{BH}} = q M_{\text{in}}$ , most strongly at  $q = 1/2$  [17, 19]. In this scenario, the critical value of  $\beta$ , above which PBHs come to dominate the Universe before fully evaporating, is significantly modified due to the memory burden effect, which prolongs the PBH lifetime.

To estimate this critical value, we assume the burden effect sets in during the inflaton-dominated era. The time at which PBHs begin to dominate is then given by  $t_{\text{BH}} \sim t_{\text{in}}(q\beta)^{-(1+w_\phi)/2w_\phi}$ . On the other hand, the PBH lifetime is given by Eq. (15), i.e.,  $t_{\text{ev}}^n = 1/\Gamma_{\text{BH}}^n$ . Equating these two timescales yields the modified critical value of  $\beta$ ,

$$\beta_c^n \sim \left[ \left( \frac{M_P}{qM_{\text{in}}} \right)^{2(n+1)} \frac{(3+2n)\epsilon}{2^{1-n}3\pi\gamma(1+w_\phi)} \right]^{\frac{2w_\phi}{1+w_\phi}} q^{-\frac{1+3w_\phi}{1+w_\phi}}. \quad (\text{B8})$$

The above expression reduces to the standard semiclassical result, Eq. (8), in the limit  $n = 0$  and  $q = 1$  (corresponding to the case without memory burden).

Let us now compute the reheating temperature for the case  $\beta < \beta_c$ , although this scenario is not the main focus of the current work. As previously discussed, for  $\beta < \beta_c$  and a small inflaton decay rate  $\Gamma_\phi \ll H$ , the universe can be reheated via PBH evaporation, which occurs after a certain time, i.e.,  $a_{\text{RH}} > a_{\text{ev}}$ . The reheating condition in this case is given by

$$\rho_{\text{RH}} = \rho_{\text{BH}}(a_{\text{ev}}) \left( \frac{a_{\text{ev}}}{a_{\text{RH}}} \right)^4 = \rho_\phi(a_{\text{in}}) \left( \frac{a_{\text{in}}}{a_{\text{RH}}} \right)^{3(1+w_\phi)}, \quad (\text{B9})$$

from which we find

$$T_{\text{RH}} = \left( \frac{48}{\alpha} \right)^{\frac{1}{4}} \left[ \frac{2^{n-1}(3+2n)\epsilon}{3(1+w_\phi)(\pi\gamma)^{3w_\phi}} \right]^{\frac{1}{2(1-3w_\phi)}} \beta^{\frac{3(1+w_\phi)}{4(3w_\phi-1)}} \times \left( \frac{M_P}{M_{\text{in}}} \right)^{\frac{3(1-w_\phi)+2n}{2(1-3w_\phi)}} q^{\frac{9+3w_\phi+4n}{4(3w_\phi-1)}} M_P, \quad (\text{B10})$$

where to find the above expression, we used  $(a_{\text{ev}}/a_{\text{RH}})^4 = (q\beta)^{4/(3w_\phi-1)}(a_{\text{in}}/a_{\text{ev}})^{12w_\phi/(1-3w_\phi)}$ . On the other hand, for  $\beta > \beta_c^n$ , the reheating temperature is determined by Eq. (17), and can be expressed as

$$T_{\text{RH}} = \left( \frac{4}{3\alpha} \right)^{\frac{1}{4}} \sqrt{\frac{2^n(3+2n)\epsilon}{q^{3+2n}}} \left( \frac{M_P}{M_{\text{in}}} \right)^{\frac{3}{2}+n} M_P. \quad (\text{B11})$$

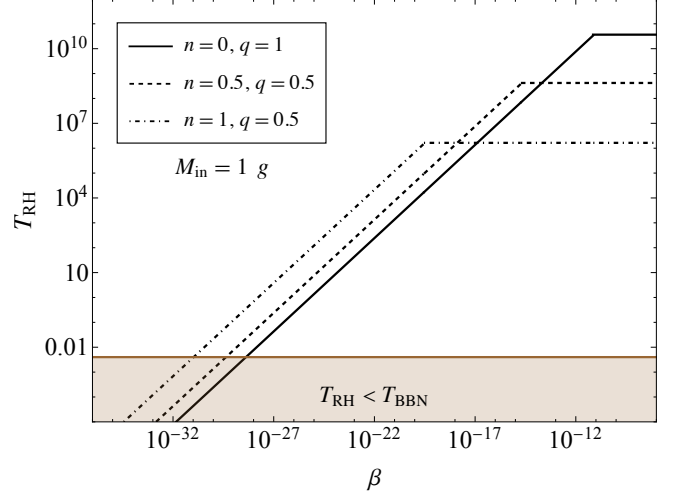


Figure 8. The reheating temperature as a function of  $\beta$  is plotted here for standard Hawking evaporation ( $n = 0, q = 1$ ) and for two different combinations of memory burden parameters: ( $n = 1/2, q = 1/2$ ) and ( $n = 1, q = 1/2$ ), represented respectively by the solid, dashed, and dot-dashed black curves.

In Fig. 8, we show how the reheating temperature varies as a function of  $\beta$ . As expected, for values  $\beta > \beta_c^n$ , which differ depending on the specific scenario, such as standard Hawking evaporation or different memory burden cases, we observe a  $\beta$ -independent plateau in the reheating temperature.

The maximum initial PBH mass that can fully evaporate before the onset of Big Bang Nucleosynthesis (BBN) can be estimated by requiring the PBH lifetime  $t_{\text{ev}}^n \sim 1$  sec, and turns out as

$$M_{\text{in}} \leq \frac{M_P}{q} [2^n(3+2n)\epsilon t_{\text{BBN}} M_P]^{\frac{1}{2n+3}} \sim \frac{1.1 \times 10^9 \text{ g}}{q} [2^n(3+2n)]^{\frac{1}{2n+3}} (1.5 \times 10^{-29})^{\frac{n}{2n+3}}. \quad (\text{B12})$$

The above equation implies that, under standard Hawking evaporation, the maximum allowed PBH formation mass is  $M_{\text{in}} \leq 1.6 \times 10^9 \text{ g}$ . However, when incorporating the memory burden effect with representative values  $q = 1/2$  and  $n = 1$ , as adopted throughout our analysis, this bound becomes significantly tighter, yielding  $M_{\text{in}} \leq 6.1 \times 10^3 \text{ g}$ . Meanwhile, constraints on the tensor-to-scalar ratio from Planck+BICEP2/Keck ( $r_{0.05} < 0.036$ ) [118, 119] imply an upper bound on the inflationary Hubble scale,  $H_{\text{I}} < 4.8 \times 10^{13} \text{ GeV}$ . This, in turn, sets a lower bound on the PBH formation mass  $M_{\text{in}} \geq 0.5 \text{ g} \left( \frac{\gamma}{0.2} \right)$ .

## 2. Hawking evaporation

The complete mass evolution of the PBH is described by a first phase of usual Hawking evaporation up to a time  $t_q$  after which it will follow the burdened evolution described by Eq. (14). overall the mass evolution can be summarized in the following form

$$M_{\text{BH}}(t) = M_{\text{in}} \left(1 - \Gamma_{\text{BH}}^{(0)}(t - t_{\text{in}})\right)^{\frac{1}{3}} \theta(t_q - t) + q M_{\text{in}} \left[1 - \Gamma_{\text{BH}}^{(n)}(t - t_q)\right]^{\frac{1}{3+2n}} \theta(t - t_q). \quad (\text{B13})$$

From there, the temperature evolution and the instantaneous emissions will be modified according to the new PBH mass evolution. The temperature will be computed in the usual way, Eq. (2) is still valid and will therefore exhibit the same "bouncing" behavior as the mass evolution. The more subtle point comes at the level of the instantaneous emission. The usual workaround for PBH evaporation is to get the generic instantaneous emission before integrating it with respect to the energy in order to get the proper mass evolution. Here we are working the other way around by imposing an extra  $S^{-n}$  suppression at the level of the mass evolution. Luckily this term does not depend on the energy which result in a rather simple modification of the instantaneous emission

$$\begin{aligned} \frac{d^2 N_{i,lm}}{dt dE} &= (\theta(t_q - t) + \frac{\theta(t - t_q)}{S^n}) \frac{1}{2\pi} \frac{\Gamma_{s_i,lm}(E, M, x_j)}{e^{E/T_{\text{BH}}} - (-1)^{2s_i}} \\ &\sim (\theta(t_q - t) + \frac{\theta(t - t_q)}{S^n}) 27\pi^2 R_S^2 \frac{g_i}{(2\pi)^3} \frac{E^2}{e^{E/T_{\text{BH}}} - (-1)^{2s_i}}, \end{aligned} \quad (\text{B14})$$

where we took the geometric optic limit in the last step. We also introduced here the greybody factor  $\Gamma_{s_i,lm}$  which encapsulates the reabsorption of the emitted particles by the PBH. Regarding the computations, we used the geometric optic limit but the figures take this factor into account since we used instantaneous emission curves from Black Hawk [120, 121] to produce our plots.

## 3. The spectrum

Let's now have a look at the shape of the PBH evaporation spectra in more details. The whole work is to properly integrate the contribution of the PBH population using the instantaneous emission relation given in Eq. (B14). The GW abundance can be reconstructed using

$$\frac{d\rho_{\text{GW}}^{\text{BH}}}{dt dk} = n_{\text{BH}}(t) k \frac{dN_i}{dt dk}. \quad (\text{B15})$$

Since the memory burden affects only the latest stage of evaporation through the mass evolution, the evaporation

can be expressed in the usual form [30]

$$\frac{d\rho_{\text{GW}}^{\text{BH}}}{d \ln k_0} = \frac{27 n_{\text{in}}^{\text{BH}} k_0^4}{64\pi^3 M_P^4} \frac{1}{S^n} \int_{a_{\text{in}}}^{a_{\text{ev}}} \frac{M_{\text{BH}}^2(a)}{\exp\left(\frac{k_0 M_{\text{BH}} a_0}{M_P^2 a}\right) - 1} \left(\frac{a_{\text{in}}}{a}\right)^3 \frac{da}{Ha}. \quad (\text{B16})$$

Here, the factor  $M_{\text{BH}}^2$  with Eq. (B13) splits the integral in two contributions from each evaporation phase, giving the 2-peaks structure of the spectra one can see in Fig. 1 at the  $D'_1$  and  $D'_2$  spots. Eq. (B16) then gives an estimation of the peak frequency if we approximate the mass of the PBH as constant before an abrupt evaporation,

$$f_{0,ev} \approx \frac{2.8}{2\pi} T_{\text{BH}} \left(\frac{a_{ev}}{a_0}\right), \quad (\text{B17})$$

which is the relation used in section VI. The evaporation scale factor  $a_{ev}$  in Eq.(B17) can either be  $a_q$  for  $D'_1$  or  $a_{RH}$  for  $D'_2$ . We can at this level grasp a fundamental difference between  $D'_1$  and  $D'_2$  since  $D'_2$  is tied to the reheating temperature which is fixed by the last stage of PBH evaporation. This peak has therefore a fixed frequency which depends only on the mass while  $D'_1$  feels on top, the redshift  $a_q/a_{RH}$  which implies a dependence on the burden parameters.

## 4. Value at the peak

Starting from Eq. (B16), we can compute the main peak value for the PBH evaporation ( $D_1$  and  $D'_2$ ). The simplest way is to express everything with respect to the reheating time while assuming the PBH mass as constant during the PBH domination era. We assume for simplicity that PBH domination occurs after the burden effect kicks in<sup>12</sup>. Under this assumption, the PBH spectra can be expressed as [30]

$$\left. \frac{d\rho}{d \ln k_0} \right|_{\beta > \beta_c} = \frac{27\sqrt{3}}{64\pi^3} \frac{k_0^{\frac{5}{2}} \sqrt{\rho_{\text{RH}}}}{S^n \sqrt{q} M_{\text{in}}} \left(\frac{a_{ev}}{a_0}\right)^{\frac{3}{2}} \times I_0^{\beta_c}, \quad (\text{B18})$$

with

$$I_0^{\beta_c} = \int_{\frac{k_0 M_{\text{in}}}{M_P^2} \frac{a_0}{a_{\text{ev}}}}^{\frac{k_0 M_{\text{in}}}{M_P^2} \frac{a_0}{a_{\text{BH}}}} \frac{\sqrt{Y}}{e^Y - 1} dY. \quad (\text{B19})$$

Note that at this stage, our relations are generic. No other assumption has been made apart from the ones mentioned above.

<sup>12</sup>The subtlety of the exact dynamic between the burdening and the domination can be technically taken into account but it only affects the tail of the spectra, which does not affect our results.

The independence of the peak with respect to the mass of the PBH is also simple to demonstrate if we focus on the term that exhibits a mass contribution. The "hidden" mass factor are present in the entropy ( $S$ ), the peak frequency ( $k_0$ ), the reheating energy density ( $\rho_{\text{RH}}$ ) and the redshift between reheating and today ( $a_{\text{ev}}/a_0$ ). By massaging a bit those contribution we get

$$\left. \frac{d\rho}{d\ln k_0} \right|_{\beta > \beta_c} \propto \frac{1}{S^n (qM_{\text{in}})^3 T_{\text{RH}}^2} \propto (qM_{\text{in}})^0. \quad (\text{B20})$$

After collecting all the constant factor, the peak amplitude for the GW spectra can be expressed<sup>13</sup>

$$\Omega_{\text{GW}}|_{\beta > \beta_c}^{\text{peak}} = \frac{81(2.8)^{5/2}}{128\pi^3(3+2n)} \frac{\alpha}{\epsilon} \left( \frac{g_0}{g_{\text{RH}}} \right)^{\frac{2}{3}} \frac{T_0^4}{3M_P^2 H_0^2} I_0^{\beta_c}. \quad (\text{B21})$$

Then, the peak value is overall the same as for the regular hawking evaporation ( $n = 0$ ,  $q = 1$ ,  $\Omega_{\text{GW}} \sim 10^{-8}$ ). We only inherit a dependency on the burden parameter  $n$  through the constant factor in front of the amplitude. For our benchmark point ( $n = 1$ ,  $q = 1/2$ ) the peak amplitude is then approximately the same up to an  $\mathcal{O}(1)$  reduction factor, which fits with Fig. 1.

### Appendix C: Inflaton scattering

After inflation, the Universe goes through a phase of oscillation of the inflaton field  $\phi$ , following an average equation of state  $P_\phi = w_\phi \rho_\phi$ , with

$$w_\phi = \frac{k-2}{k+2}, \quad (\text{C1})$$

for a potential [69, 70]

$$V(\phi) = \lambda M_P^4 \left( \frac{\phi}{M_P} \right)^k. \quad (\text{C2})$$

This potential can be seen as the limit  $\phi \ll M_P$  of, for instance, a Starobinsky potential [122] of the form

$$V(\phi) = \frac{3}{4} m_\phi^2 M_P^2 \left( 1 - e^{-\sqrt{\frac{2}{3}} \frac{\phi}{M_P}} \right)^2, \quad (\text{C3})$$

or  $\alpha$ -attractor T-models [123]

$$V(\phi) = \lambda M_P^4 \left[ \sqrt{6} \tanh \left( \frac{\phi}{\sqrt{6} M_P} \right) \right]^k. \quad (\text{C4})$$

The evolution of a dominant  $\phi$ -energy density is expressed in the Boltzmann equation

$$\dot{\rho}_\phi + 3(1+w_\phi)H\rho_\phi \simeq 0, \quad (\text{C5})$$

which implies

$$\rho_\phi = V(\phi_0) = \rho_{\text{end}} \left( \frac{a_{\text{end}}}{a} \right)^{3(1+w_\phi)} = \rho_{\text{end}} \left( \frac{a_{\text{end}}}{a} \right)^{\frac{6k}{k+2}}, \quad (\text{C6})$$

with  $\rho_{\text{end}}$  being the inflaton energy density at the end of inflation. As for the field  $\phi$ , it obeys the equation of motion

$$\ddot{\phi} + 3H\dot{\phi} + \frac{dV}{d\phi} \approx 0. \quad (\text{C7})$$

The solution to this equation can be parametrized as

$$\phi(t) = \Phi(t) \underbrace{\sum_{\nu} \mathcal{P}_\nu(t)}_{\mathcal{P}} e^{-i\nu\omega t}, \quad (\text{C8})$$

where  $\Phi$  is the envelope of the field and the  $\mathcal{P}_\nu$  are the Fourier coefficients of the quasi periodic oscillatory function  $\mathcal{P}$ . Since we have a separation of scales between the fast oscillating scale ( $\mathcal{O}(m_\phi)$ ) and the slower expansion of the universe ( $\mathcal{O}(H)$ ) we can decompose Eq. (C7) as [69–71]

$$\ddot{\Phi} = -\frac{6H}{n+2}\Phi, \quad (\text{C9})$$

$$\dot{\mathcal{P}}^2 = \frac{2m_\phi^2}{k(k-1)}(1 - \mathcal{P}^k). \quad (\text{C10})$$

Solving this set of equations leads to a decaying envelope  $\Phi$  and a oscillating frequency  $\omega$  of the form

$$\Phi \propto a^{-\frac{6}{k+2}}, \quad (\text{C11})$$

$$\omega = m_\phi \sqrt{\frac{\pi k}{2(k-1)} \frac{\Gamma(\frac{1}{2} + \frac{1}{k})}{\Gamma(\frac{1}{k})}}, \quad (\text{C12})$$

where the inflaton effective mass is defined with the usual convention,  $m_\phi = \sqrt{V''(\Phi)}$ . From this decomposition, the inflaton can be seen as an infinite sum of modes with energies  $E = \nu\omega$  with a decreasing amplitude  $\Phi_\nu = \Phi \mathcal{P}_\nu$ .

Regarding the gravitational waves produced by the inflaton scattering, it is more convenient to develop  $V(\phi) \sim \phi^k$  in harmonics since they appear in the vertices for the relevant diagrams. We denote them  $(\mathcal{P}^k)_n$ . The rate of energy transfer between the inflaton and the gravitational waves can then be expressed as [67]

$$(1+w_\phi)\Gamma_h \rho_\phi = \frac{\rho_\phi^2 \omega}{4\pi M_P^4} \Sigma^k, \quad (\text{C13})$$

<sup>13</sup>note that here there is an extra 1/2 difference compared to [30] due to a slight difference in the convention of the reheating temperature

with

$$\Sigma^k = \sum_{\nu=1}^{\infty} \Sigma_{\nu}^k \equiv \sum_{\nu=1}^{\infty} \nu |(\mathcal{P}^k)_{\nu}|^2. \quad (\text{C14})$$

Finally, the gravitational waves spectra can be written, for  $k \neq 4$  [30]

$$\begin{aligned} \Omega_{GW} h^2 &= \frac{h^2}{\rho_c^0} \frac{d\rho_{GW}^{\phi}(a_0)}{df_0} = \frac{h^2}{\rho_c^0} \frac{1}{a_0^4} \frac{d[a^4 \rho_{GW}^{\phi}(a)]}{df_0} \\ &= \frac{h^2}{\rho_c^0} \frac{\sqrt{3} \rho_{\text{end}}^{3/2}}{4M_P^3} \frac{k+2}{|k-4|} \left( \frac{2\pi}{\omega_{\text{end}}} \right)^{\frac{3k-3}{k-4}} \left( \frac{a_0}{a_{\text{end}}} \right)^{\frac{9}{k-4}} \Sigma^k f_0^{\frac{4k-7}{k-4}}. \end{aligned} \quad (\text{C15})$$

Note that Eq. (C15) does not hold for  $k = 4$ , since in this case the inflaton energy scale  $\omega$ , redshifts as fast as the radiation it produces. This can be seen by computing the relation giving today's frequency of a graviton produced at a scale factor  $a$ ,

$$\begin{aligned} f_0(a) &= \frac{\omega(a)}{2\pi} \frac{a}{a_0} \\ &= \frac{\gamma_k}{2\pi} M_P \left( \frac{\rho_{\text{end}}}{M_P^4} \right)^{\frac{k-2}{2k}} \left( \frac{a_{\text{end}}}{a} \right)^{\frac{3k-6}{k+2}} \left( \frac{a}{a_0} \right). \end{aligned} \quad (\text{C16})$$

This relation grasps most of the physics needed to understand the shape of the spectrum. Indeed, if  $k = 4$  this relation clearly show a constant frequency, independent on  $a$ . This gives a a dirac shaped spectrum<sup>14</sup>. It is consistent with the idea that, in this case, the Universe should not the reheating transition since the equation of state is kept unchanged before and after reheating. On the other hand, for  $k > 4$ , the frequency behaves as some negative power law of the scale factor resulting in a spectra growing with  $f_0$  since then later produced graviton have an overall smaller frequency.

## Appendix D: GW from density fluctuations

### 1. Generalities

Scalar induced gravitational waves have been shown to be an exciting possibility to probe early Universe scenarios especially in the context of PBH reheating due to

the sharp transition to radiation domination [31, 76, 79–81, 84, 85, 124]. The appendix presented here stands more as a lightning introduction to get to our main result which is the analytic relation for the scalar induced

<sup>14</sup>In fact a forest of spectra peaked at  $\nu\omega$ .

gravitational waves for a burdened PBH with an arbitrary initial equation of state presented in Eq. (D19) and (D20). This extends the recent results of [80, 81], while also shedding light on the issue of non-linearity which sets the cutoff of the spectra seen in figure 1. For a more detailed analysis on the formalism, we redirect the reader to a proper review<sup>15</sup> [83]. Starting from the perturbed metric

$$ds^2 = (1 - 2\Phi)dt^2 - a^2(\tau) [(1 + 2\Phi)\delta_{ij} + h_{ij}]dx^i dx^j, \quad (\text{D1})$$

the tensor modes are sourced at second order by scalar fluctuations [76, 81, 83], whose equation of motion is

$$h''_{k,\lambda} + 2\mathcal{H}h'_{k,\lambda} + k^2 h_{k,\lambda} = \mathcal{S}_{k,\lambda}, \quad (\text{D2})$$

where the source term  $\mathcal{S}$  can be expressed as

$$\mathcal{S}_{k,\lambda} = 4 \int \frac{d^3q}{(2\pi)^3} e_{\lambda}^{ij}(\mathbf{k}) q_i q_j \Phi_{\mathbf{q}} \Phi_{|\mathbf{k}-\mathbf{q}|} f(\tau, q, |\mathbf{k}-\mathbf{q}|), \quad (\text{D3})$$

with

$$\begin{aligned} f(\tau, q, |\mathbf{k}-\mathbf{q}|) &= T_{\Phi}(q\tau) T_{\Phi}(|\mathbf{k}-\mathbf{q}|\tau) \\ &\quad + \frac{2}{3(1+w)} \left( T_{\Phi}(q\tau) + \frac{T'_{\Phi}(q\tau)}{\mathcal{H}} \right) \\ &\quad \left( T_{\Phi}(|\mathbf{k}-\mathbf{q}|\tau) + \frac{T'_{\Phi}(|\mathbf{k}-\mathbf{q}|\tau)}{\mathcal{H}} \right). \end{aligned} \quad (\text{D4})$$

Solving the evolution of the scalar potential accounting for the cosmological evolution, the gravitational wave signal during radiation domination can be expressed as [76, 81, 83]

$$\Omega_{GW}(k) = \frac{k^2}{12\mathcal{H}^2} \overline{\mathcal{P}_h(k, \tau)}, \quad (\text{D5})$$

with the tensorial power spectrum expressed as [127]

<sup>15</sup>Note that modifications of gravity or loop corrections can also have impact on the background of gravitational waves [125, 126].

$$\bar{\mathcal{P}}_h \approx \frac{c_s^4}{8} \left( \frac{\mathcal{H}}{k} \right)^2 \left( \frac{k}{k_{eva}} \right)^8 \int_0^\infty dv \int_{|1-v|}^{1+v} du \left( 4v^2 - (1+v^2-u^2)^2 \right)^2 \bar{\mathcal{I}}_{\text{osc}}^2 P_\Phi(uk) P_\Phi(vk) S_\Phi^2(uk) S_\Phi^2(vk) \mathcal{T}_\Phi^2(uk) \mathcal{T}_\Phi^2(vk). \quad (\text{D6})$$

The functions  $S_\Phi$  are phenomenological suppression factors which take into account how the scalar potential decay during the transition to radiation domination and  $\mathcal{P}_\Phi$  is the initial power spectra which in our case come from [76] :

$$\mathcal{P}_\Phi(k) = \frac{2}{3\pi} \left( \frac{k}{k_{UV}} \right)^3. \quad (\text{D7})$$

In Eq. (D7),  $k_{UV}$  is the scale related to PBH formation, introduced in Eqs. (68) and (76). From Eqs. (D5) and (D6), we can then redshift the GW abundance

$$\Omega_{\text{GW},0}(k) h^2 \approx 0.387 \left( \frac{g_*(T_{\text{RH}})}{106.75} \right)^{-1/3} \Omega_{r,0} h^2 \Omega_{\text{GW},\text{RD}}(k). \quad (\text{D8})$$

## 2. The spectrum

Before diving in the details of the spectrum for the unburdened case, we should introduce specific ratio of scales that allow to simplify the expressions:

$$\frac{k_{UV}}{k_{\text{in}}} = \left( \frac{\beta}{\gamma} \right)^{\frac{1}{3}}, \quad (\text{D9})$$

$$\frac{k_{\text{BH}}}{k_{\text{in}}} = \sqrt{2} \beta^{\frac{1+3w_\phi}{6w_\phi}}, \quad (\text{D10})$$

$$\frac{k_{\text{RH}}}{k_{\text{in}}} = \left( \frac{\beta \epsilon}{2\pi \gamma} \frac{M_{\text{P}}^2}{M_{\text{in}}^2} \right)^{\frac{1}{3}}. \quad (\text{D11})$$

From there, following [81] the GW spectra today can be expressed as the sum of two contributions,

$$\Omega_{\text{GW},\text{res}}^{\text{peak}} = C^4(w) \frac{c_s^{7/3} (c_s^2 - 1)^2}{576 \times 6^{1/3} \pi} \left( \frac{k_{\text{BH}}}{k_{UV}} \right)^8 \times \left( \frac{k_{UV}}{k_{\text{RH}}} \right)^{17/3} \left( \frac{k}{k_{UV}} \right)^{\frac{11}{3}}, \quad (\text{D12})$$

$$\Omega_{\text{GW},\text{IR}}(k) = C^4(w) \frac{c_s^4}{120\pi^2} \left( \frac{2}{3} \right)^{1/3} \left( \frac{k_{\text{BH}}}{k_{UV}} \right)^8 \times \left( \frac{k_{UV}}{k_{\text{RH}}} \right)^{14/3} \left( \frac{k}{k_{UV}} \right). \quad (\text{D13})$$

These two contributions are visible on the unburdened curve of Fig. 1, but even more clear through the break in the shaded spectrum in Fig. 9, where the cutoff constraint has been released. Note also that we introduced  $C(w)$ , which is a numerical constant determined by the matching of the scalar fluctuations transfer function between the inflaton domination and the PBH domination era. Its exact definition is given by [81]

$$C(w) = \frac{9}{20} \alpha_{\text{fit}}^{-\frac{1}{3w}} \left( 3 + \frac{1-3w}{1+3w} \right)^{-\frac{1}{3w}}, \quad (\text{D14})$$

where  $\alpha_{\text{fit}} \approx 0.135$  is a numerically determined constant.

## 3. Burdening the spectrum

Moving to the burdened spectrum, the overall physics is the same. The memory burden effect mainly affects *when* the PBHs decay and the duration of the evaporation. This induces modifications of the scale  $k_{\text{eva}}$  and the suppression factor. Following [80], we get

$$\frac{k_{\text{RH}}}{k_{\text{in}}} = \left[ \frac{((3+2k)2^n \epsilon)^2}{36\pi^2 \gamma^2} \left( \frac{M_{\text{in}}}{M_{\text{P}}} \right)^2 \left( \frac{M_{\text{P}}}{q M_{\text{in}}} \right)^{6+4n} \beta^2 \right]^{\frac{1}{6}}, \quad (\text{D15})$$

and

$$S_{\Phi,\text{eva}}(k) = q \left( \frac{2}{\sqrt{3}} \frac{\kappa}{\sqrt{3\kappa-1}} \frac{k}{k_{\text{RH}}} \right)^{-\frac{1}{3\kappa}}, \quad (\text{D16})$$

where  $\kappa$  is a function of  $n$  introduced by convenience as

$$\kappa = 1 + \frac{2n}{3}. \quad (\text{D17})$$

With this new variable, taking the unburdened limit  $n = 0$  and  $q = 1$  corresponds to  $\kappa = 1$ , for which we can



check that the above expressions converge to the unburdened case.

Finally, the last missing piece is the transfer function for the fluctuations which is

$$\mathcal{T}_\Phi(k) = \left( 5 + \frac{1}{C(w)} \left( \frac{k}{k_{\text{BH}}} \right)^2 \right)^{-1}. \quad (\text{D18})$$

The shape of this transfer function causes the calculation to be divided between the IR and UV contributions. Modes respecting  $k \gg k_{\text{BH}}$  which are the ones which re-entered before PBH domination, are damped due to the pressure of the inflaton fluid that limit the growth of the fluctuations. On the other hand, the ones entering during PBH domination ( $k \ll k_{\text{BH}}$ ) should not experience this effect.

With this in mind, using Eq. (D6) and following appendix D and E of [81], the GW spectra during radiation domination can be expressed as in the previous case, by the sum of two contributions

$$\Omega_{\text{GW, res}}(k) = \frac{(2c_s)^2 \frac{2^{3\kappa+2}}{3\kappa} C^4(w) q^4 (c_s^2 - 1)^2}{13824 c_s \pi} \left( \kappa \sqrt{\frac{2}{3}} \sqrt{\frac{2}{3\kappa - 1}} \right)^{-\frac{4}{3\kappa}} \left( \frac{k}{k_{\text{UV}}} \right)^{5 - \frac{4}{3\kappa}} \left( \frac{k_{\text{UV}}}{k_{\text{RH}}} \right)^{7 - \frac{4}{3\kappa}} \left( \frac{k_{\text{BH}}}{k_{\text{UV}}} \right)^8 \Theta_{\text{UV}}(k), \quad (\text{D19})$$

and

$$\Omega_{\text{GW, IR2}} = \frac{C_s^4 C(w)^4 q^4}{36\pi^2} \frac{\kappa}{9\kappa - 4} \left( \sqrt{\frac{2}{3}} \frac{\kappa \sqrt{2}}{\sqrt{3\kappa - 1}} \right)^{-\frac{4}{3\kappa}} \left( \frac{k_{\text{BH}}}{k_{\text{RH}}} \right)^8 \left( \frac{k_{\text{RH}}}{k_{\text{UV}}} \right)^{\frac{6\kappa+4}{3\kappa}} \left( \frac{k}{k_{\text{UV}}} \right). \quad (\text{D20})$$

As for the previous equations the spectrum converges to Eqs. (D13) and (D12) in the unburdened limit and reproduces the previous results existing in the literature [80, 81].

#### 4. Non-linear cutoff

As highlighted in [79–81], during the period of PBH domination, fluctuations grow over time as described by the Poisson equation

$$\Phi = \frac{3}{2} \left( \frac{\mathcal{H}}{k} \right)^2 \delta_{\text{PBH}}. \quad (\text{D21})$$

The initial power spectrum of the fluctuations in Eq. (D7), approaches unity when the momentum approaches  $\sim k_{\text{UV}}$ . Consequently, the spectrum (D19) may overestimate GW production for momenta larger than

a certain nonlinear scale  $k_{\text{NL}}$  that we need to estimate. This scale is defined as the scale where  $\delta_{\text{PBH}} \sim 1$ , based on the Poisson equation. Since the relevant quantity is the fluctuations during radiation domination, we must evolve the fluctuations until PBH evaporation, using the transfer function from Eq. (D18), and a suppression factor arising from the smooth nature of PBH decay [81]. Collecting all the expressions, the non linear cutoff should then satisfy the condition

$$k_{\text{NL, sup}} \sim k_{\text{BH}} \sqrt{\frac{5C(w)}{\frac{2C(w)}{3} \left( \frac{k_{\text{BH}}}{k_{\text{RH}}} \right)^2 S_\Phi \Phi_{\text{init}} - 1}}. \quad (\text{D22})$$

A good approximation for this scale comes from the pole inside the square root, while estimating  $\Phi_{\text{init}} \sim \sqrt{\mathcal{P}_\Phi}$

$$k_{\text{NL, sup}} \sim k_{\text{UV}} \left( \frac{3}{2C(w)q} \sqrt{\frac{3\pi}{2}} \left( \frac{2\kappa}{\sqrt{9\kappa - 3}} \right)^{\frac{1}{3\kappa}} \left( \frac{k_{\text{eva}}}{k_{\text{eq}}} \right)^2 \left( \frac{k_{\text{UV}}}{k_{\text{eva}}} \right)^{\frac{1}{3\kappa}} \right)^{\frac{6\kappa}{9\kappa - 2}}. \quad (\text{D23})$$

For completeness we can also compute the non-linear scale without the suppression factor which is a more conservative statement

$$k_{\text{NL}} \sim \left( \sqrt{\frac{3\pi}{2}} \frac{3}{2C(w)} \right)^{\frac{2}{3}} \left( \frac{k_{\text{eva}}}{k_{\text{eq}}} \right)^{\frac{4}{3}} k_{\text{UV}}. \quad (\text{D24})$$

In all the figures presented above, we choosed to stay conservative using Eq. (D24). To let the reader appreciate the impact of the cutoff scale, we reproduce the Fig. 1 while using different cutoffs with shaded curves in Fig. 9.

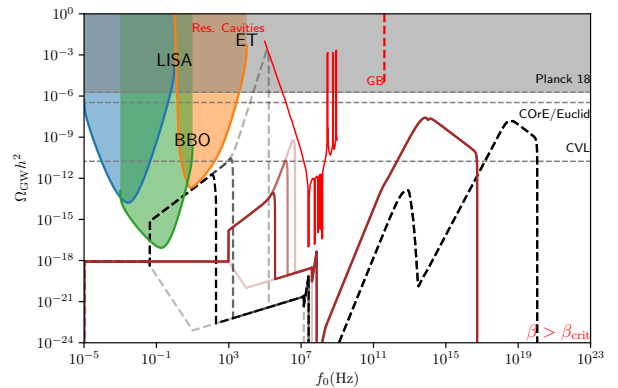


Figure 9. Fig. 1 with different cutoffs. For each color, going from left to right, the most opaque is using  $k_{\text{cut}} = k_{\text{NL}}$  from Eq. (D24), then the intermediate is using  $k_{\text{cut}} = k_{\text{NL}}$  from Eq. (D23) and the most shaded is using  $k_{\text{cut}} = k_{\text{UV}}$  from Eq. (76).

- 
- [1] B. P. Abbott et al. (LIGO Scientific, Virgo), *Phys. Rev. Lett.* **116**, 061102 (2016), [arXiv:1602.03837 \[gr-qc\]](#).
- [2] B. P. Abbott et al. (LIGO Scientific, Virgo), *Phys. Rev. X* **6**, 041015 (2016), [Erratum: *Phys. Rev. X* **8**, 039903 (2018)], [arXiv:1606.04856 \[gr-qc\]](#).
- [3] B. P. Abbott et al. (LIGO Scientific, Virgo), *Annalen Phys.* **529**, 1600209 (2017), [arXiv:1608.01940 \[gr-qc\]](#).
- [4] B. P. Abbott et al. (LIGO Scientific, VIRGO), *Phys. Rev. Lett.* **118**, 221101 (2017), [Erratum: *Phys. Rev. Lett.* **121**, 129901 (2018)], [arXiv:1706.01812 \[gr-qc\]](#).
- [5] R. Abbott and A. et al., *Physical Review D* **104** (2021), [10.1103/physrevd.104.022004](#).
- [6] B. P. Abbott et al. (LIGO Scientific, Virgo), *Phys. Rev. Lett.* **119**, 141101 (2017), [arXiv:1709.09660 \[gr-qc\]](#).
- [7] B. P. Abbott et al. (LIGO Scientific, Virgo), *Astrophys. J. Lett.* **851**, L35 (2017), [arXiv:1711.05578 \[astro-ph.HE\]](#).
- [8] S. Hild et al., *Class. Quant. Grav.* **28**, 094013 (2011), [arXiv:1012.0908 \[gr-qc\]](#).
- [9] P. Amaro-Seoane et al. (LISA), (2017), [arXiv:1702.00786 \[astro-ph.IM\]](#).
- [10] G. Agazie et al. (NANOGrav), *Astrophys. J. Lett.* **951**, L8 (2023), [arXiv:2306.16213 \[astro-ph.HE\]](#).
- [11] G. Agazie et al. (NANOGrav), *Astrophys. J. Lett.* **951**, L9 (2023), [arXiv:2306.16217 \[astro-ph.HE\]](#).
- [12] J. Antoniadis et al. (EPTA), *Astron. Astrophys.* **678**, A48 (2023), [arXiv:2306.16224 \[astro-ph.HE\]](#).
- [13] J. Antoniadis et al. (EPTA, InPTA:), *Astron. Astrophys.* **678**, A50 (2023), [arXiv:2306.16214 \[astro-ph.HE\]](#).
- [14] A. Zic et al., *Publ. Astron. Soc. Austral.* **40**, e049 (2023), [arXiv:2306.16230 \[astro-ph.HE\]](#).
- [15] D. J. Reardon et al., *Astrophys. J. Lett.* **951**, L6 (2023), [arXiv:2306.16215 \[astro-ph.HE\]](#).
- [16] M. Riajul Haque, E. Kpatcha, D. Maity, and Y. Mambrini, *Phys. Rev. D* **108**, 063523 (2023), [arXiv:2305.10518 \[hep-ph\]](#).
- [17] A. Alexandre, G. Dvali, and E. Koutsangelas, *Phys. Rev. D* **110**, 036004 (2024), [arXiv:2402.14069 \[hep-ph\]](#).
- [18] G. Dvali, J. S. Valbuena-Bermúdez, and M. Zantedeschi, *Phys. Rev. D* **110**, 056029 (2024), [arXiv:2405.13117 \[hep-th\]](#).
- [19] V. Thoss, A. Burkert, and K. Kohri, *Mon. Not. Roy. Astron. Soc.* **532**, 451 (2024), [arXiv:2402.17823 \[astro-ph.CO\]](#).
- [20] J. Crowder and N. J. Cornish, *Phys. Rev. D* **72**, 083005 (2005), [arXiv:gr-qc/0506015](#).
- [21] V. Corbin and N. J. Cornish, *Class. Quant. Grav.* **23**, 2435 (2006), [arXiv:gr-qc/0512039](#).
- [22] M. Maggiore et al. (ET), *JCAP* **03**, 050 (2020), [arXiv:1912.02622 \[astro-ph.CO\]](#).
- [23] B. Sathyaprakash et al., *Class. Quant. Grav.* **29**, 124013 (2012), [Erratum: *Class. Quant. Grav.* **30**, 079501 (2013)], [arXiv:1206.0331 \[gr-qc\]](#).
- [24] A. Abac et al., (2025), [arXiv:2503.12263 \[gr-qc\]](#).
- [25] F. R. Bouchet et al. (CoRE), (2011), [arXiv:1102.2181 \[astro-ph.CO\]](#).
- [26] R. Laureijs et al. (EUCLID), (2011), [arXiv:1110.3193 \[astro-ph.CO\]](#).
- [27] I. Ben-Dayan, B. Keating, D. Leon, and I. Wolfson, *JCAP* **06**, 007 (2019), [arXiv:1903.11843 \[astro-ph.CO\]](#).
- [28] M. R. Haque, E. Kpatcha, D. Maity, and Y. Mambrini, *Phys. Rev. D* **109**, 023521 (2024), [arXiv:2309.06505 \[hep-ph\]](#).
- [29] B. Barman, S. Jyoti Das, M. R. Haque, and Y. Mambrini, *Phys. Rev. D* **110**, 043528 (2024), [arXiv:2403.05626 \[hep-ph\]](#).
- [30] M. Gross, Y. Mambrini, E. Kpatcha, M. O. Olea-Romacho, and R. Roshan, *Phys. Rev. D* **111**, 035020 (2025), [arXiv:2411.04189 \[hep-ph\]](#).
- [31] D. Paul, M. R. Haque, and S. Pal, (2025), [arXiv:2503.18207 \[astro-ph.CO\]](#).
- [32] S. Balaji, G. Domènech, G. Franciolini, A. Ganz, and J. Tränkle, *JCAP* **11**, 026 (2024), [arXiv:2403.14309 \[gr-qc\]](#).
- [33] D. Qiu, S. Jiang, and F. P. Huang, (2025), [arXiv:2508.04314 \[hep-ph\]](#).
- [34] W.-Y. Ai, (2025), [arXiv:2508.02794 \[hep-ph\]](#).
- [35] J. Gunn, Impacts of Primordial Black Holes in the Early Universe, Ph.D. thesis, Naples U. (2025), [arXiv:2503.14583 \[hep-ph\]](#).
- [36] K. Kohri, “Overview on Current Constraints on the Primordial Black Hole Abundance,” (2025).
- [37] M. R. Haque, S. Maity, D. Maity, and Y. Mambrini, *JCAP* **07**, 002 (2024), [arXiv:2404.16815 \[hep-ph\]](#).
- [38] S. W. Hawking, *Nature* **248**, 30 (1974).
- [39] S. W. Hawking, *Commun. Math. Phys.* **43**, 199 (1975), [Erratum: *Commun. Math. Phys.* **46**, 206 (1976)].
- [40] J. H. MacGibbon and B. R. Webber, *Phys. Rev. D* **41**, 3052 (1990).
- [41] J. Auffinger, I. Masina, and G. Orlando, *Eur. Phys. J. Plus* **136**, 261 (2021), [arXiv:2012.09867 \[hep-ph\]](#).
- [42] I. Masina, *Grav. Cosmol.* **27**, 315 (2021), [arXiv:2103.13825 \[gr-qc\]](#).
- [43] A. Cheek, L. Heurtier, Y. F. Perez-Gonzalez, and J. Turner, *Phys. Rev. D* **105**, 015022 (2022), [arXiv:2107.00013 \[hep-ph\]](#).
- [44] A. Arbey, M. Calzà, and Y. F. Perez-Gonzalez, *Phys. Dark Univ.* **48**, 101903 (2025), [arXiv:2502.17240 \[gr-qc\]](#).
- [45] S. Das, M. R. Haque, J. Kalita, R. Karmakar, and D. Maity, (2025), [arXiv:2505.15419 \[astro-ph.CO\]](#).
- [46] S. Maity, (2025), [arXiv:2507.02821 \[astro-ph.CO\]](#).
- [47] G. Dvali, (2018), [arXiv:1810.02336 \[hep-th\]](#).
- [48] G. Dvali, L. Eisemann, M. Michel, and S. Zell, *JCAP* **03**, 010 (2019), [arXiv:1812.08749 \[hep-th\]](#).
- [49] G. Dvali, M. Zantedeschi, and S. Zell, (2025), [arXiv:2503.21740 \[hep-ph\]](#).
- [50] G. Dvali, L. Eisemann, M. Michel, and S. Zell, *Phys. Rev. D* **102**, 103523 (2020), [arXiv:2006.00011 \[hep-th\]](#).
- [51] A. Chaudhuri, K. Kohri, and V. Thoss, (2025), [arXiv:2506.20717 \[astro-ph.CO\]](#).
- [52] A. Takeshita and T. Kitabayashi, (2025), [arXiv:2506.20071 \[hep-ph\]](#).
- [53] X.-h. Tan and Y.-f. Zhou, (2025), [arXiv:2505.19857 \[astro-ph.CO\]](#).
- [54] M. Chianese, (2025), [arXiv:2504.03838 \[astro-ph.HE\]](#).
- [55] P. Athron, M. Chianese, S. Datta, R. Samanta, and N. Saviano, *JCAP* **05**, 005 (2025), [arXiv:2411.19286](#)

- [astro-ph.CO].
- [56] M. Chianese, A. Boccia, F. Iocco, G. Miele, and N. Saviano, (2024), [arXiv:2410.07604 \[astro-ph.HE\]](#).
- [57] A. K. Saha, A. Singh, P. Parashari, and R. Laha, (2024), [arXiv:2409.10617 \[astro-ph.CO\]](#).
- [58] R. Calabrese, M. Chianese, and N. Saviano, *Phys. Rev. D* **111**, 083008 (2025), [arXiv:2501.06298 \[hep-ph\]](#).
- [59] D. Borah and N. Das, *JCAP* **02**, 031 (2025), [arXiv:2410.16403 \[hep-ph\]](#).
- [60] M. C. Guzzetti, N. Bartolo, M. Liguori, and S. Matarrese, *Riv. Nuovo Cim.* **39**, 399 (2016), [arXiv:1605.01615 \[astro-ph.CO\]](#).
- [61] K. Saikawa and S. Shirai, *JCAP* **05**, 035 (2018), [arXiv:1803.01038 \[hep-ph\]](#).
- [62] A. Chakraborty, S. Clery, M. R. Haque, D. Maity, and Y. Mambrini, (2025), [arXiv:2503.21877 \[gr-qc\]](#).
- [63] Y. Ema, R. Jinno, and K. Nakayama, *JCAP* **09**, 015 (2020), [arXiv:2006.09972 \[astro-ph.CO\]](#).
- [64] R. Tito D’Agnolo and S. A. R. Ellis, *JHEP* **04**, 164 (2025), [arXiv:2412.17897 \[gr-qc\]](#).
- [65] V. Domcke, S. A. R. Ellis, and J. Kopp, *Phys. Rev. D* **111**, 035031 (2025), [arXiv:2409.06462 \[hep-ph\]](#).
- [66] N. Aggarwal et al., (2025), [arXiv:2501.11723 \[gr-qc\]](#).
- [67] G. Choi, W. Ke, and K. A. Olive, *Phys. Rev. D* **109**, 083516 (2024), [arXiv:2402.04310 \[hep-ph\]](#).
- [68] K. Kaneta, S. M. Lee, and K.-y. Oda, *JCAP* **09**, 018 (2022), [arXiv:2206.10929 \[astro-ph.CO\]](#).
- [69] M. A. G. Garcia, K. Kaneta, Y. Mambrini, and K. A. Olive, *Phys. Rev. D* **101**, 123507 (2020), [arXiv:2004.08404 \[hep-ph\]](#).
- [70] M. A. G. Garcia, K. Kaneta, Y. Mambrini, and K. A. Olive, *JCAP* **04**, 012 (2021), [arXiv:2012.10756 \[hep-ph\]](#).
- [71] M. A. G. Garcia, K. Kaneta, Y. Mambrini, K. A. Olive, and S. Verner, *JCAP* **03**, 016 (2022), [arXiv:2109.13280 \[hep-ph\]](#).
- [72] S. Clery, Y. Mambrini, K. A. Olive, and S. Verner, *Phys. Rev. D* **105**, 075005 (2022), [arXiv:2112.15214 \[hep-ph\]](#).
- [73] S. Clery, Y. Mambrini, K. A. Olive, A. Shkerin, and S. Verner, *Phys. Rev. D* **105**, 095042 (2022), [arXiv:2203.02004 \[hep-ph\]](#).
- [74] B. Barman, S. Cléry, R. T. Co, Y. Mambrini, and K. A. Olive, *JHEP* **12**, 072 (2022), [arXiv:2210.05716 \[hep-ph\]](#).
- [75] S. Cléry, P. Anastasopoulos, and Y. Mambrini, *JCAP* **12**, 035 (2024), [arXiv:2307.06011 \[hep-ph\]](#).
- [76] T. Papanikolaou, V. Vennin, and D. Langlois, *JCAP* **03**, 053 (2021), [arXiv:2010.11573 \[astro-ph.CO\]](#).
- [77] T. Papanikolaou, *Journal of Cosmology and Astroparticle Physics* **2022**, 089 (2022).
- [78] H. Assadullahi and D. Wands, *Physical Review D* **79** (2009), 10.1103/physrevd.79.083511.
- [79] K. Inomata, M. Kawasaki, K. Mukaida, T. Terada, and T. T. Yanagida, *Phys. Rev. D* **101**, 123533 (2020), [arXiv:2003.10455 \[astro-ph.CO\]](#).
- [80] S. Balaji, G. Domènech, G. Franciolini, A. Ganz, and J. Tränkle, *Journal of Cosmology and Astroparticle Physics* **2024**, 026 (2024).
- [81] G. Domènech and J. Tränkle, (2024), [arXiv:2409.12125 \[gr-qc\]](#).
- [82] G. Domènech, C. Lin, and M. Sasaki, *JCAP* **04**, 062 (2021), [Erratum: *JCAP* **11**, E01 (2021)], [arXiv:2012.08151 \[gr-qc\]](#).
- [83] G. Domenech, *Universe* **7**, 398 (2021).
- [84] K. Inomata, K. Kohri, T. Nakama, and T. Terada, *Physical Review D* **100** (2019), 10.1103/physrevd.100.043532.
- [85] N. Bhaumik, M. R. Haque, R. K. Jain, and M. Lewicki, *Journal of High Energy Physics* **2024** (2024), 10.1007/jhep10(2024)142.
- [86] B. J. Carr, T. Harada, and H. Maeda, *Class. Quant. Grav.* **27**, 183101 (2010), [arXiv:1003.3324 \[gr-qc\]](#).
- [87] E. Babichev, V. Dokuchaev, and Y. Eroshenko, *J. Exp. Theor. Phys.* **100**, 528 (2005), [arXiv:astro-ph/0505618](#).
- [88] L. A. Boyle and P. J. Steinhardt, *Phys. Rev. D* **77**, 063504 (2008), [arXiv:astro-ph/0512014](#).
- [89] Y. Watanabe and E. Komatsu, *Phys. Rev. D* **73**, 123515 (2006), [arXiv:astro-ph/0604176](#).
- [90] C. Caprini and D. G. Figueroa, *Class. Quant. Grav.* **35**, 163001 (2018), [arXiv:1801.04268 \[astro-ph.CO\]](#).
- [91] N. Bernal and F. Hajkarim, *Phys. Rev. D* **100**, 063502 (2019), [arXiv:1905.10410 \[astro-ph.CO\]](#).
- [92] M. R. Haque, D. Maity, T. Paul, and L. Sriramkumar, *Phys. Rev. D* **104**, 063513 (2021), [arXiv:2105.09242 \[astro-ph.CO\]](#).
- [93] S. Maity and M. R. Haque, *JCAP* **04**, 091 (2025), [arXiv:2407.18246 \[astro-ph.CO\]](#).
- [94] B. Barman, A. Ghoshal, B. Grzadkowski, and A. Socha, (2023), [arXiv:2305.00027 \[hep-ph\]](#).
- [95] R. Jinno, T. Moroi, and K. Nakayama, *Phys. Rev. D* **86**, 123502 (2012), [arXiv:1208.0184 \[astro-ph.CO\]](#).
- [96] T. Louis et al. (ACT), (2025), [arXiv:2503.14452 \[astro-ph.CO\]](#).
- [97] E. Calabrese et al. (ACT), (2025), [arXiv:2503.14454 \[astro-ph.CO\]](#).
- [98] M. Kawasaki, K. Kohri, and N. Sugiyama, *Phys. Rev. Lett.* **82**, 4168 (1999), [arXiv:astro-ph/9811437](#).
- [99] M. Kawasaki, K. Kohri, and N. Sugiyama, *Phys. Rev. D* **62**, 023506 (2000), [arXiv:astro-ph/0002127](#).
- [100] T. Hasegawa, N. Hiroshima, K. Kohri, R. S. L. Hansen, T. Tram, and S. Hannestad, *JCAP* **12**, 012 (2019), [arXiv:1908.10189 \[hep-ph\]](#).
- [101] M. R. Haque, D. Maity, and P. Saha, *Phys. Rev. D* **102**, 083534 (2020), [arXiv:2009.02794 \[hep-th\]](#).
- [102] M. R. Haque and D. Maity, *Phys. Rev. D* **107**, 043531 (2023), [arXiv:2201.02348 \[hep-ph\]](#).
- [103] A. Escrivà, C. Germani, and R. K. Sheth, *JCAP* **01**, 030 (2021), [arXiv:2007.05564 \[gr-qc\]](#).
- [104] J. C. Hidalgo, L. A. Urena-Lopez, and A. R. Liddle, *Phys. Rev. D* **85**, 044055 (2012), [arXiv:1107.5669 \[astro-ph.CO\]](#).
- [105] J. Martin, T. Papanikolaou, and V. Vennin, *JCAP* **01**, 024 (2020), [arXiv:1907.04236 \[astro-ph.CO\]](#).
- [106] D. Hooper, G. Krnjaic, and S. D. McDermott, *JHEP* **08**, 001 (2019), [arXiv:1905.01301 \[hep-ph\]](#).
- [107] D. Hooper, G. Krnjaic, J. March-Russell, S. D. McDermott, and R. Petrossian-Byrne, (2020), [arXiv:2004.00618 \[astro-ph.CO\]](#).
- [108] A. Arbey and J. Auffinger, *Eur. Phys. J. C* **79**, 693 (2019), [arXiv:1905.04268 \[gr-qc\]](#).
- [109] I. Baldes, Q. Decant, D. C. Hooper, and L. Lopez-Honorez, *JCAP* **08**, 045 (2020), [arXiv:2004.14773 \[astro-ph.CO\]](#).
- [110] B. J. Carr and S. W. Hawking, *Mon. Not. Roy. Astron. Soc.* **168**, 399 (1974).

- [111] I. Musco and J. C. Miller, *Class. Quant. Grav.* **30**, 145009 (2013), [arXiv:1201.2379 \[gr-qc\]](#).
- [112] I. Musco, J. C. Miller, and A. G. Polnarev, *Class. Quant. Grav.* **26**, 235001 (2009), [arXiv:0811.1452 \[gr-qc\]](#).
- [113] I. Hawke and J. M. Stewart, *Class. Quant. Grav.* **19**, 3687 (2002).
- [114] J. C. Niemeyer and K. Jedamzik, *Phys. Rev. Lett.* **80**, 5481 (1998), [arXiv:astro-ph/9709072](#).
- [115] A. Escrivà and A. E. Romano, *JCAP* **05**, 066 (2021), [arXiv:2103.03867 \[gr-qc\]](#).
- [116] A. Escrivà, *Phys. Dark Univ.* **27**, 100466 (2020), [arXiv:1907.13065 \[gr-qc\]](#).
- [117] A. Escrivà, *Universe* **8**, 66 (2022), [arXiv:2111.12693 \[gr-qc\]](#).
- [118] P. A. R. Ade et al. (BICEP, Keck), *Phys. Rev. Lett.* **127**, 151301 (2021), [arXiv:2110.00483 \[astro-ph.CO\]](#).
- [119] P. A. R. Ade et al. (BICEP2, Planck), *Phys. Rev. Lett.* **114**, 101301 (2015), [arXiv:1502.00612 \[astro-ph.CO\]](#).
- [120] A. Arbey and J. Auffinger, *The European Physical Journal C* **79**, 693 (2019), [arXiv:1905.04268 \[astro-ph, physics:gr-qc, physics:hep-ph\]](#).
- [121] A. Arbey and J. Auffinger, *The European Physical Journal C* **81**, 910 (2021), [arXiv:2108.02737 \[astro-ph, physics:gr-qc, physics:hep-ph, physics:hep-th\]](#).
- [122] A. A. Starobinsky, *Phys. Lett. B* **91**, 99 (1980).
- [123] R. Kallosh and A. Linde, *JCAP* **07**, 002 (2013), [arXiv:1306.5220 \[hep-th\]](#).
- [124] K. Inomata, K. Kohri, T. Nakama, and T. Terada, *Phys. Rev. D* **100**, 043532 (2019), [arXiv:1904.12879 \[astro-ph.CO\]](#).
- [125] A. Addazi, A. S. Koshelev, S. Pi, and A. Tokareva, *JCAP* **06**, 017 (2025), [arXiv:2408.04004 \[gr-qc\]](#).
- [126] M. B. Fröb, D. Glavan, P. Meda, and I. Sawicki, (2025), [arXiv:2504.02609 \[astro-ph.CO\]](#).
- [127] J. Espinosa, D. Racco, and A. Riotto, *Journal of Cosmology and Astroparticle Physics* **2018**, 012–012 (2018).